Petrography, Geochemistry, and Geochronology of Cretaceous Porphyry Intrusives near Red Lodge, Montana

---

A Senior Honors Thesis Presented to

The Faculty of the Department of Earth and Atmospheric Sciences

University of Houston

In Partial Fulfillment

Of the Requirements for the Degree

Bachelor of Science

Geology

By

Logan French

May 2020

Acknowledgements

I would like to start off by thanking Barry Shaulis for his preliminary geochronology work as well as Manuel Paez-Reyes, John Byrd, Spruce Schoenemann and John Boyle for collecting the first samples which created a starting point for this paper. My work collecting samples was possible thanks to Greg Creasey for letting me stay at the YBRA cabins a few extra days. Thank you to Weiyao Yan and Dr. John Casey for helping me with the initial geochemistry work and offering me their machines and advice. Thank you to Dr. Tom Kalakay for our numerous conversations concerning the geology of the Beartooth Mountains during which he provided helpful sources to investigate as well as his expertise on the region. Minako Righter was helpful and kind throughout the process of my research and helped me through the geochronology process. Lastly, I would like to thank Dr. Tom Lapen and Dr. Jinny Sisson. Tom helped guide me through the process leading up to and after my U-Pb analysis and frequently gave advice towards my project. Jinny helped me with virtually all aspects of the project from giving me the opportunity to work on it to advising me on the best software for geochemical analysis. Thank you to all who have helped me in this process.

Petrography, Geochemistry, and Geochronology of Cretaceous Porphyry Intrusives near Red Lodge, Montana

---

An Abstract of Senior Honors Thesis

Presented to

The Faculty of the Department of Earth and Atmospheric Science

University of Houston

In Partial Fulfillment

Of the Requirements for the Degree

Bachelor of Science

Geology

By Logan French

May 2020

Abstract

There are many localities of Cretaceous porphyry intrusives in and around the Beartooth Range and particularly along the Beartooth Front near Red Lodge, Montana. Although Rouse et al. (1937) carried out a study devoted to them, they have been almost ignored since then and today new methods are available in order to further our understanding of their history. In recent decades, there has been some confusion as to the age of these rocks due to their proximity to Paleogene porphyry felsic to intermediate intrusives. In contrast, Cretaceous porphyry intrusive rocks represent intrusion prior to the main Laramide thrusting of the region. These are felsic porphyries ranging in composition from andesite to dacite and all have large plagioclase phenocrysts with prominent zoning. The initial geochemical data suggests that these intrusives are the result of fractional crystallization. Geologic observations of the region have shown through relative geochronology that these rocks are late Cretaceous in age and this has been confirmed by preliminary geochronology by Barry Shaulis which provided an age of 93 Ma, and by this study which yielded an age of 96.7 +/- 1.77 Ma.

Table of Contents

Acknowledgements iii

Abstract v

Table of Contents vi

1 Introduction 1

1.1 Overview 1

1.2 Regional Geologic Context and Literature Review 1

1.2.1 Geologic History and Structures 1

1.2.2 Igneous Activity 5

1.2.3 Relevant Sedimentary Units 8

1.3 Motivation for Study 10

2 Sampling and Analytical Methods 12

2.1 Locations and Petrography 12

2.1.1 Red Lodge Front 15

2.1.2 Switchbacks 18

2.1.3 Summary 20

2.2 Isotopic Geochronology 21

2.2.1 Preliminary Research from Shaulis 21

2.3 Geochemical Techniques 25

3 Results and Discussion 25

3.1 U-Pb Geochronology 25

3.2 Geochemistry 28

3.3 Regional Relations ad Cross Section 38

4 Conclusion 43

5 Bibliography 44

1 Introduction

1.1 Overview

This research project focuses on U-Pb geochronology, geochemistry, and petrography of andesite porphyry dikes sampled near the Yellowstone Bighorn Research Association (YBRA) field station near Red Lodge, Montana. My samples were collected near the Beartooth Thrust Fault (also known as the Beartooth Front) as well as near the northeastern corner of the Beartooth Mountains. This region in and around Red Lodge and the Beartooth Mountains in Montana is adjacent to Yellowstone National Park, making it the focus of many geologic studies. However, andesitic intrusions in this region have not been studied in many decades. The older studies lacked the technology and regional context that is accessible today. Because these dikes were injected into overlying units, they can be used to constrain the timing of tectonic activity. Determining the age of these features creates a better understanding of their geologic relation to the other units and the Laramide thick-skinned fold and thrust belt.

1.2 Regional Geologic Context and Literature Review

1.2.1 Geologic History and Structures

As shown in Figure 1, Red Lodge is just to the northeast of the Beartooth Mountains, which form a part of the central Rocky Mountains (Dutcher et al., 1986). The Beartooth Mountains consists of a Precambrian crystalline core and are the most northerly of several blocks created by uplift and thrusting during the Laramide orogeny surrounding the Bighorn Basin in

south-central Montana and northwestern Wyoming (Poldevaart and Bentley, 1958; Foose, 1958; Dutcher et al., 1986; Wise, 2000). The range is approximately 80 miles long by 20 miles wide with a northwest-southeast orientation stretching from Clark, Wyoming to north of Nye, Montana (Dutcher et al., 1986; Poldevaart and Bentley, 1958; Foose, 1958; Spencer, 1958; Wise, 2000).

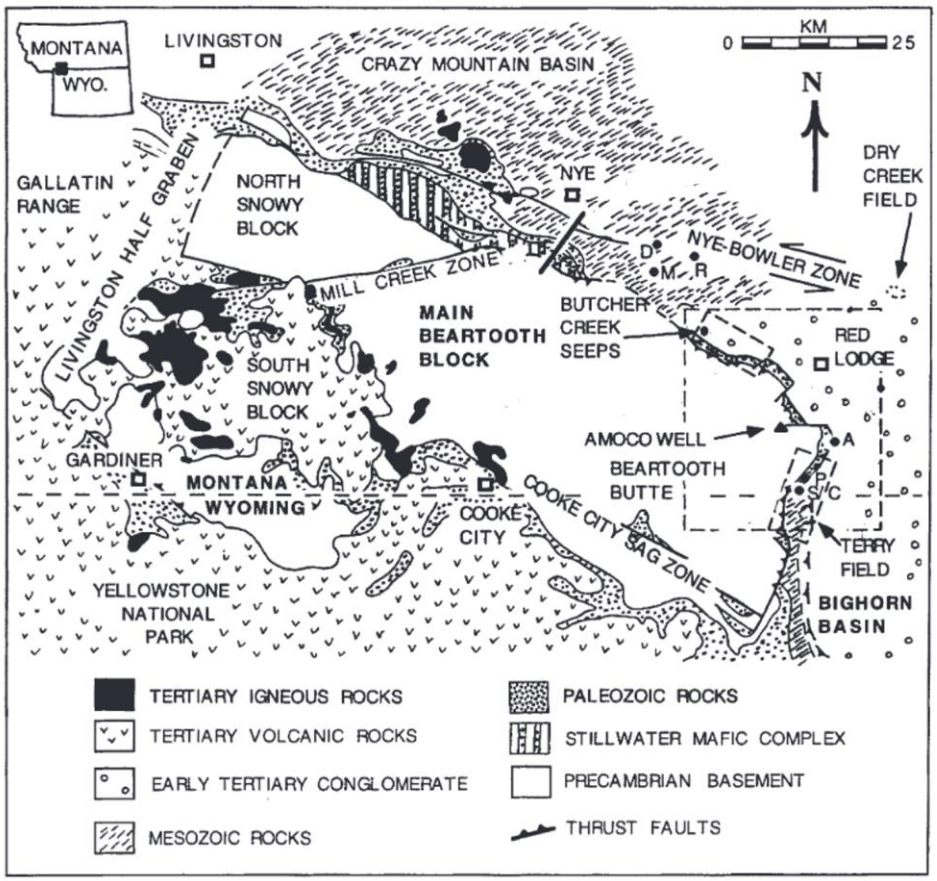

Figure 1 Tectonic features of the greater Beartooth uplift. D = Dean dome, M = Mackay dome, P = Phillips Ruby A well, A = Amoco Burlington Northern well, R = Roscose dome, S/C = Shell/Carter Line Ditch well. (modified from Wise, 2000) The dashed box indicates the area of study shown in Figure 2.

During the Precambrian, the region was metamorphosed, deformed followed by intrusion of felsic magmas and then basaltic dikes (Foose, 1958; Eckelmann and Poldevaart, 1957). The folding, dike injection, and related fractures mainly trend NW-SE which influenced deformation patterns much later during the Laramide orogeny (Foose, 1958; Eckelmann and Poldevaart, 1957).

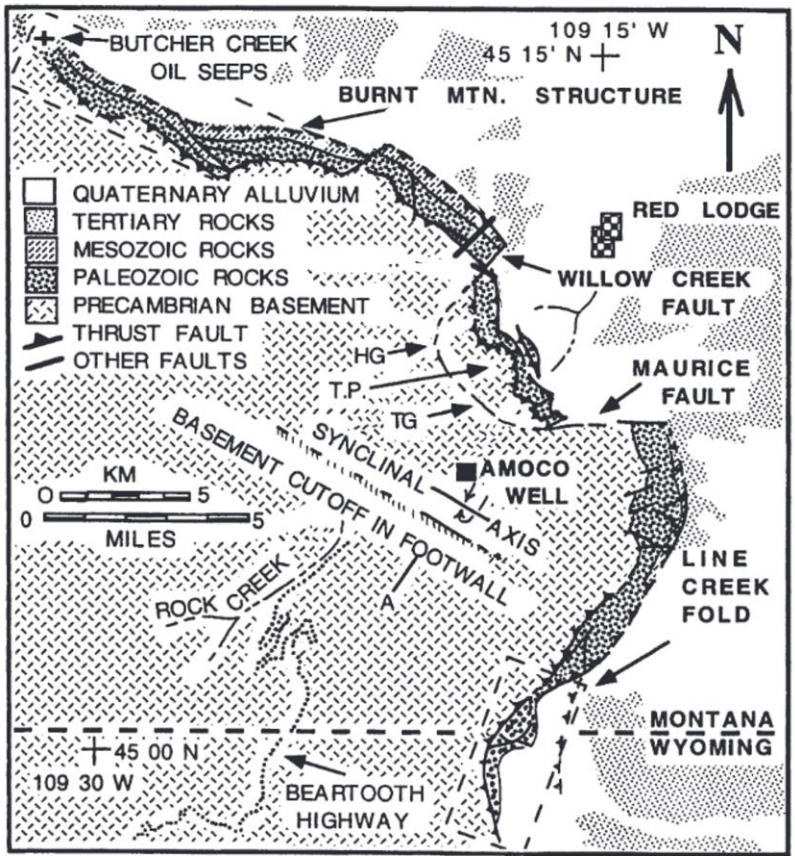

Figure 2 Structural features associated with the Red Lodge corner of the Beartooth uplift (mountain front data after Foose et al. (1961), modified from Wise (2000)). TP = Towne Point, TG = Towne Gulch, HG = Hayward Gulch.

Subsequently, the area experienced both marine and terrestrial deposition and was generally tectonically inactive from the Paleozoic to the mid Cretaceous (Rouse et al., 1937; Foose, 1958; Spencer, 1958). At this point, deformation started during the Laramide orogeny (Rouse et al., 1937; Foose, 1958). The Beartooth Front, a thrust fault with a west and southwest dip along the east and northeast edges of the Beartooth Mountains, formed and thrust the Precambrian basement rocks over Cretaceous and Tertiary rocks during the Laramide orogeny (Foose, 1958; Spencer, 1958; Dutcher et al., 1986; DeCelles et al., 1991). Thrusting occurred during and after Paleocene time (Parsons, 1958). The Beartooth Fault produced and eventually cut through a large fault-propagation fold, thrusting Precambrian crystalline rocks over part of

the Bighorn Basin and creating peaks along the east and northeast sides and a gentle slope to the southwest (Foose 1958; DeCelles et al., 1991; Omar et al., 1994; Carrapa et al., 2019). The edges of the uplift commonly exhibit nearly vertical Phanerozoic units which were thrusted, folded, and eroded (Figure 3). The Precambrian basement peaks stand at about 4,000 to 5,000 feet higher than the surrounding topography, giving the range a maximum elevation of about 10,000 feet (Foose, 1958; Wise, 2000).

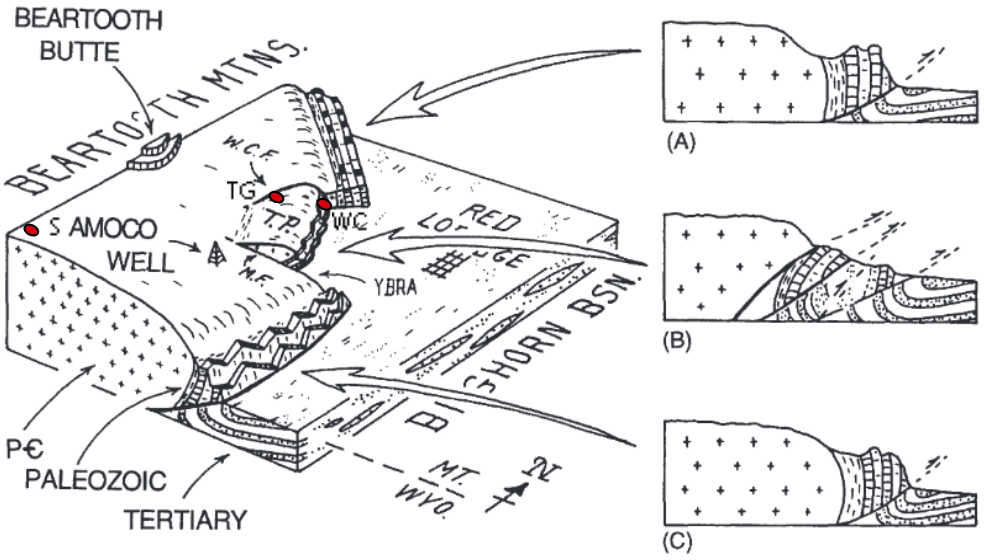

Figure 3 Block diagram of structures at the Red Lodge corner of the Beartooth Front (modified from Wise (2000)). Red dots represent my sample locations. WCF = Willow Creek fault, MF = Maurice fault, TP = Towne Point.

During the Laramide orogeny, conglomerate, sandstone, siltstone, and mudstone units were formed in response to the uplift and deposited on the northeastern and eastern flanks of the Beartooth Mountains (Dutcher et al., 1986). These rocks are most visible today along the northwestern edge of the Beartooth Mountains from Clark's Fork of the Yellowstone River to near Red Lodge (Dutcher et al., 1986).

The Nye-Bowler lineament (Nye-Bowler zone in Figure 1) is a series of asymmetric synclines and anticlines associated with two fault systems stretching from the Beartooth Mountains through the Bighorn Basin, and into the Pryor Mountains (Foose, 1958). Movement along this fault occurred as the Fort Union Formation was being deposited, creating a difference in stratigraphic thickness on the north and south side of the fault (Spencer, 1958; Foose et al., 1986).

The Stillwater complex (Figure 1) is a tilted differentiated ultramafic/mafic pluton exposed along the northern side of the Beartooth Mountains (Poldevaart and Bentley, 1958; Jones et al., 1960). It intruded into early Archean gneisses and metasedimentary units to the south during the late Archean. To the north, it is unconformably overlain by middle Cambrian sedimentary units.

1.2.2 Igneous Activity

There are two periods of igneous activity in the Absaroka-Beartooth Region that are of interest in this study: these occurred in the late Cretaceous and those intruded in the Paleogene. The units formed in the late Cretaceous include the Livingston volcanics, the Sliderock Mountain volcano, the Independence volcanics from the Absaroka Range, Southwest Montana Batholiths, and the porphyry intrusives from this study. Their composition is intermediate to felsic (Rouse et al., 1937; Parsons, 1958). They were emplaced during early Laramide time prior to major thrusting and are associated with the Nye-Bowler lineament (Rouse et al., 1937; Parsons, 1942; Parsons, 1958). Igneous activity during the Paleogene include the Absaroka-Yellowstone volcanics, the Big Timber Stock of the Crazy Mountains, and younger porphyry intrusives

(Rouse et al., 1937; Parsons, 1958). These rocks tend to be intermediate to mafic and were emplaced during and after the main Laramide thrusting (Rouse et al., 1937; Parsons, 1942).

The Livingston Group is a felsic volcanic series including intrusives, extrusives, breccias, and pyroclastics which grade laterally into volcanic sandstones and conglomerates and then Cretaceous sediment (Parsons, 1942; Parsons, 1958). Plant fossil material in these pyroclastics are Upper Cretaceous, equivalent to the Judith River Formation that was deposited between 80 and 75 Ma (Parsons, 1942).

The Sliderock Mountain Volcano is an Upper Cretaceous stratovolcano located between the Crazy Mountains Basin and the Beartooth Mountains and is a part of the first period of igneous activity and is associated with the Nye-Bowler Lineament (Du Bray and Harlan, 1998). Its composition ranges from basaltic andesite to dacite.

The Absaroka-Yellowstone Volcanics are a thick volcanic series created during the Paleocene that lie adjacent to, and partially cover, the southwest edge of the Beartooth Mountains (Foose, 1958; Parsons, 1958; Rubel, 1971).

Porphyry intrusives can be found in several locations throughout the Beartooth Mountains area (Figure 4). They occur along the northeastern flank of the range and most intruded into the Cambrian Gros Ventre shales (Rouse et al., 1936; Foose, 1958; Dutcher et al., 1986). Relatively small sheet-like intrusions outcrop within roughly vertical Cambrian shales three miles southwest of Red Lodge and at Line Creek. These were offset by the Willow Creek tear fault shown in Figures 1, 2, and 3 (Dutcher et al., 1986). Half of a mile north of Line Creek lies a large laccolith at least 1,000 feet across on the Beartooth Plateau (Dutcher et al., 1986). Along the westward extension of the Nye-Bowler lineament several sizeable laccoliths and sills

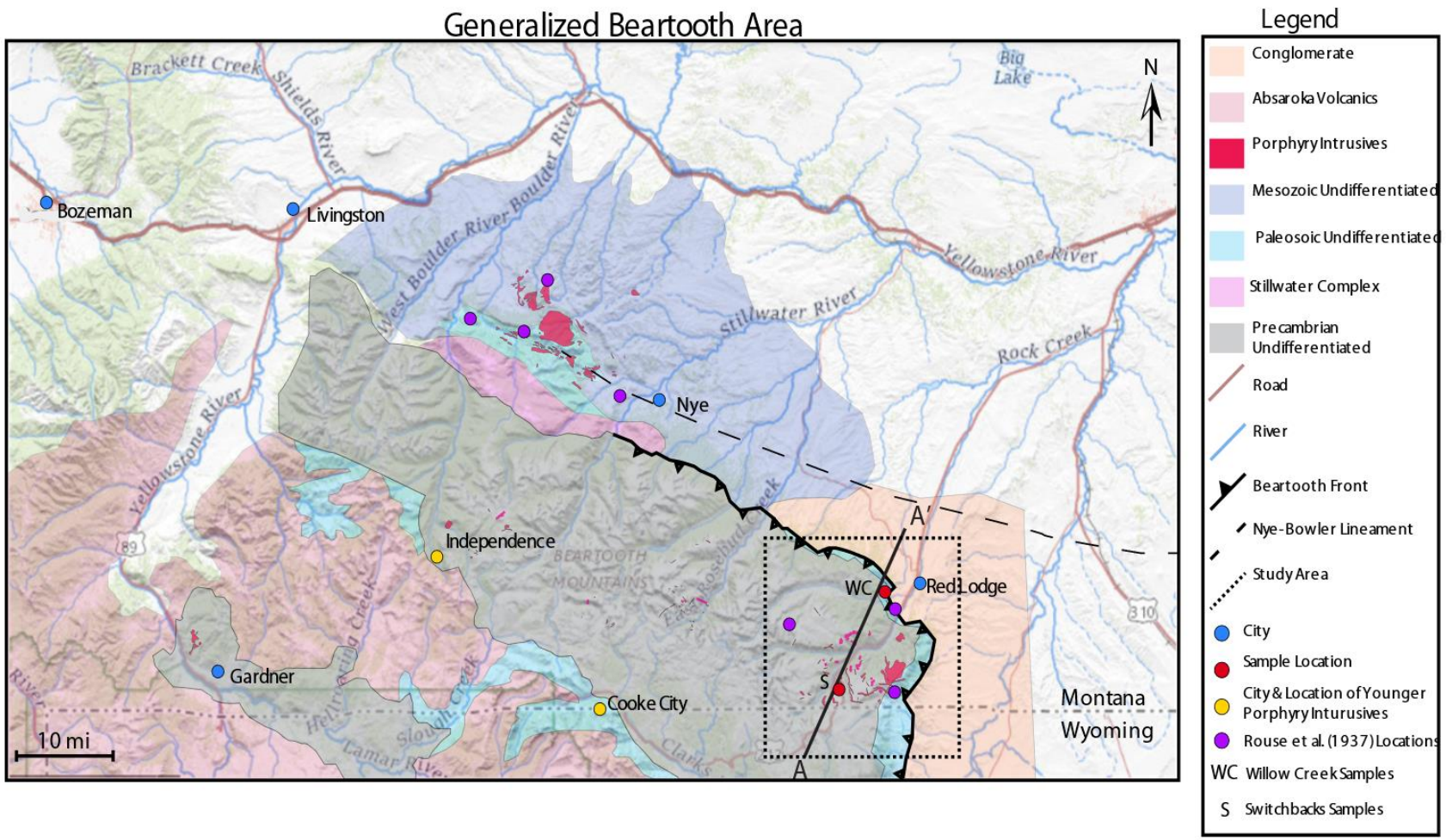

Figure 4 Generalized Map of the Beartooth Area

outcrop (Foose, 1958; Dutcher et al., 1986). Commonly, these porphyry intrusives are grouped together with porphyritic rhyolite, dacite, quartz latite, and diorite (Rouse et al., 1937; Lopez, 2005; Van Gosen et al., 2000).

1.2.3 Relevant Sedimentary Units

There are several conglomerate units which contain clasts of andesite porphyry including the Livingston Group, Linley Conglomerate, Frontier Formation, Beartooth Conglomerate and unnamed conglomerates in Gold Creek and Bennett Creek. These are synorogenic deposits which were carried and dropped by a system of alluvial fans, a coarse braided fluvial system, and swamp deposits which transported sediment basinward from the Beartooth Front (Duthcer et al., 1986; DeCelles et al., 1991; Lopez, 2005).

The Livingston Group is overlain by the Fort Union Formation (Jobling and Dutcher, 1972; Jobling 1974). Part of the proximal facies of the Fort Union Formation include conglomerates with clasts compositions including Paleozoic limestones, igneous and metamorphic rock fragments, and andesite porphyry in a coarse sand matrix (Dutcher et al., 1986).

The Linley Conglomerate is a member of the Fort Union Formation (Lopez, 2005). The Fort Union formation overlies the Cretaceous Livingston Group and its proximal facies include a pebble conglomerate with clasts of andesite porphyry, Paleozoic limestone, and igneous and metamorphic rock fragments in a coarse sand matrix (Dutcher et al., 1986). The lower Linley conglomerate contains a minor amount of andesite porphyry clasts (Dutcher et al., 1986). The middle and proximal facies of the Linley Conglomerate, however includes clasts of andesite

porphyry rocks as a major constituent (Dutcher et al., 1986; Jobling and Ritter, 1986). Dutcher et al. (1986) interpreted these clasts to be from the younger group of andesite porphyry rocks studied by Rouse et al. (1937) but they do not provide an explanation as to why. This interpretation is problematic as the Linley Conglomerate was deposited on the northeastern side of the Beartooth Mountains, rather than the western side, where Rouse et al. (1937) said that the younger porphyries are found. Dutcher et al. (1986) found that, generally, the abundance of andesite porphyry clasts increases upward (basinward) and towards the northeast. The andesite porphyry clasts tend to occur as well rounded, medium to coarse grains and are commonly more altered than other lithic clasts (Dutcher et al., 1986). Geochronology techniques have failed to give an exact age to the conglomerate, but it is generally considered to be Paleocene in age, although an Eocene age has not been entirely ruled out (Dutcher et al., 1986).

The Frontier formation has conglomerates made up of mostly felsite porphyry pebbles (Foose et al., 1986). Pebble conglomerates in Gold Creek also have clasts of the younger intrusives. Conglomerates in Bennet Creek also have the younger porphyry clasts (Rouse et al., 1937; Foose et al., 1986). The Beartooth Conglomerate is an Upper Paleocene conglomerate located along the eastern edge of the Beartooth Mountains (DeCelles et al., 1991). The Gold Creek exposure includes conglomerates with clasts of older porphyries (Foose et al., 1986).

Based on the spread of porphyry intrusives and clasts in conglomerates, a greater percentage of the rocks were transported east of the Beartooth range, while a smaller amount were deposited to the southeast around Bennet Creek or northwest and southwest near Rock Creek (Dutcher et al., 1986). These conglomerate units are interpreted as alluvial fan deposits consisting of clasts which originated in the Beartooth Mountains (Dutcher et al., 1986).

1.3 Motivation for Study

Work by Rouse et al. (1937) used relative geochronology techniques in order to better understand the age of the porphyries and their petrology. Conglomerates of the Wasatch beds contain clasts of these rocks. Their study proved that most of them were formed prior to the Wasatch period.

Although mentioned in some subsequent studies (e.g., Poldevaart and Bentley, 1958; Foose, 1958; Parsons, 1958; Spencer, 1958; Jones et al., 1960; Catanzaro and Kulp, 1963; Rubel, 1971; Lopez, 2005), these Cretaceous porphyry intrusives were last studied several decades ago and their geologic history could thus be improved by using present day research techniques. There is very limited information on these dikes, however, they are usually assumed to be Paleocene in age and younger than the Beartooth Conglomerate created by the Laramide Orogeny (Rouse, 1937; Parsons, 1958; Stobbe, 1952). It has also been suggested that they are related to the previously mentioned felsic volcanic rock activity of Independence Volcano (Rouse, 1937; Rubel, 1971). The only readily available research on these andesite porphyry dikes appears to be from Rouse et al. in 1937 which posits that they are more likely older than the Beartooth thrust fault and therefore the Beartooth Conglomerate. Apart from this, most sources that mention the porphyry intrusives of the region cite Rouse et al (1937) when discussing the age.

As mentioned in the previous section, many of the porphyries intruded into the area along the Red Lodge Front which underwent deformation in the form of folding and faulting during the Laramide Orogeny. Despite this, the intrusives here maintain their composition, texture, and thickness throughout and occur in a sheet-like form parallel to bedding planes (Rouse et al., 1937). They are also displaced along several tear faults in the area. They likely intruded into the

incompetent Gros Ventre shale after their ascent through older layers prior to thrusting along the Front (Rouse et al., 1937).

Porphyries near Nye and MacLeod also suggest intrusion prior to deformation based on laccoliths. They must be at least as young as the late Cretaceous as they occur in Upper Cretaceous stratigraphic units in some areas around Nye (Rouse et al., 1937).

Rouse et al. (1937) asserts that the porphyries started their ascent prior to thrusting in the northern and eastern regions of the Beartooth Mountains in response to the bulging of the Beartooth Mountains just before the thrusting. This "bulging" is not an emplacement mechanism favored today. The structure of the intrusives was mostly determined by pre-existing structures such as the Nye-Bowler lineament. However, the southern region of the Beartooth Mountains, around the Mill Creek area show intrusion of porphyries after the thrusting creating a series of younger porphyries nearby to the south west of the older porphyries (Rouse et al., 1937). This likely lead to some of the age confusion in other sources. The younger intrusives are not the focus of this study, but they are important to mention as they help to build up a geologic picture and explain previous confusion. These were intruded along the steep faults which mark the southern boundary of the Beartooth block (Wilson, 1936; Rouse et al., 1937). Although the younger porphyry intrusives did commonly follow steep faults, no porphyries intruded along thrust faults due to the environment of compression (Rouse et al., 1937). These younger porphyries have a much larger range in composition and are intermediate to mafic in origin (Rouse et al., 1937).

Although much of the geology in and around YBRA has been heavily studied, research on these dikes is fragmented. It is usually assumed that they were injected in the Paleocene and are younger than the Beartooth Conglomerate created by the Laramide Orogeny (e.g., Lopez et

al., 2005). Alternatively, Rouse et al. (1937) posits that the andesite porphyry dikes are more likely late Cretaceous in age based on extensive relative geochronology, making it older than the Beartooth thrust fault. Recently Barry Shaulis completed an initial U-Pb analysis using laser ablation which produced a preliminary age of about 93 million years old, which reinforces the hypothesis of Rouse et al. (Shaulis, personal communication to Sisson, 2018). Because of these contradictory theories and general lack of study, we found it necessary to further analyze these dikes and continue Shaulis' work.

2 Sampling and Analytical Methods

2.1 Locations and Petrography

The samples studied in this paper were collected from a variety of locations around the Beartooth Front during July 2018 and July 2019. The two primary locations are the Red Lodge Front and the Switchbacks, shown in Figures 4 and 5. The Red Lodge Front samples include those taken near Willow Creek (WC) and near Towne Gulch (TG). The Switchbacks (S) includes samples collected from Switchbacks 1, Quad Creek, and the Scenic Overlook. Figure 6 shows both hand samples and thin section examples for each of my sample locations. The top row (A, B, and C) and from Willow Creek. All other rows are from various locations along the Switchbacks.

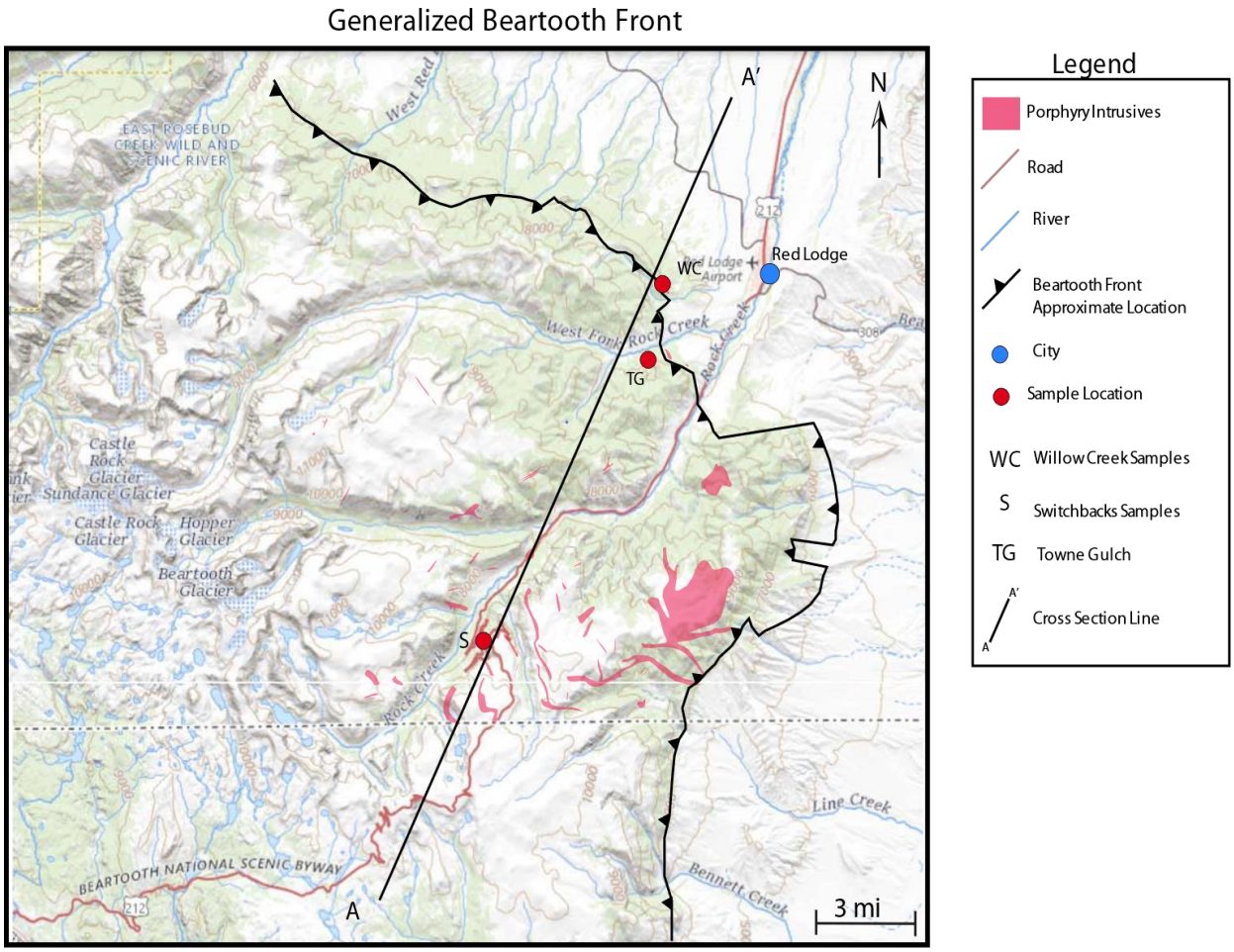

Figure 5 Generalized map of the Beartooth Front Area. Geologic contacts and structures are based on maps from Rouse et al. (1937), Wise (2000), and Van Gosen et al. (2000).

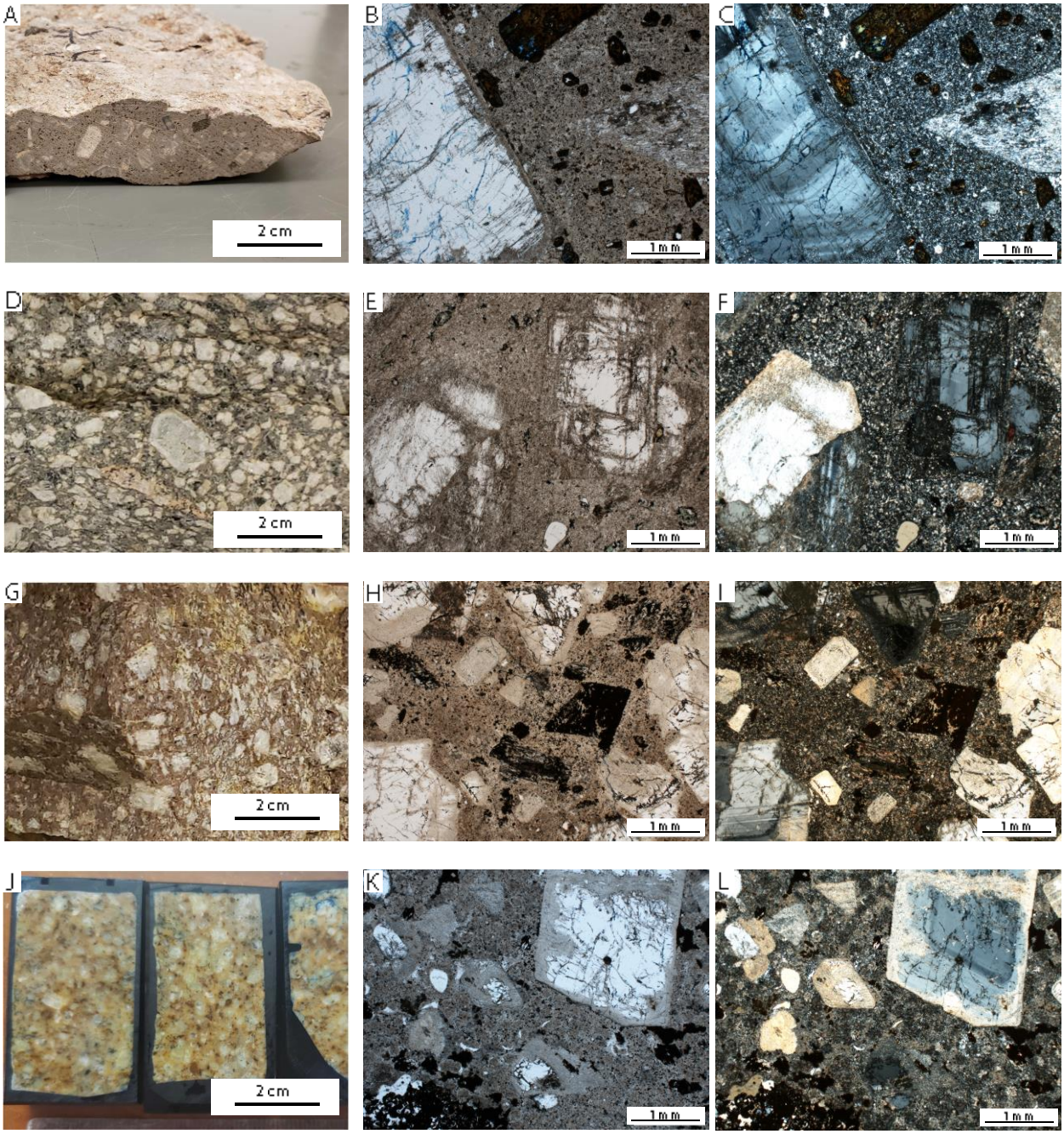

Figure 6 Examples of samples in both hand sample and thin section. From left to right, the columns are hand samples, thin sections in PPL, thin sections in XPL. From top the bottom the rows are Willow Creek samples, Switchbacks 1, Switchbacks 2, and ABP.

2.1.1 Red Lodge Front

Samples from the Red Lodge Front (Figure 7) were collected by Barry Shaulis near Towne Gulch, Manuel Paez Reyes, John Boyle, and Spruce Schoenemann on July 23, 2018 near Willow Creek and by Logan French on July 8, 2019 near Willow Creek. This area is the same as the "Red Lodge Front" described in Rouse et al. (1937). Samples from Shaulis' study were not available to me but based on descriptions from him and Rouse et al. (1937), they should be very similar to the Willow Creek samples. In this location, the porphyry occurs as a continuous sheet-like body intruding the Gros Ventre shale (Cambrian) and has been offset by the Willow Creek

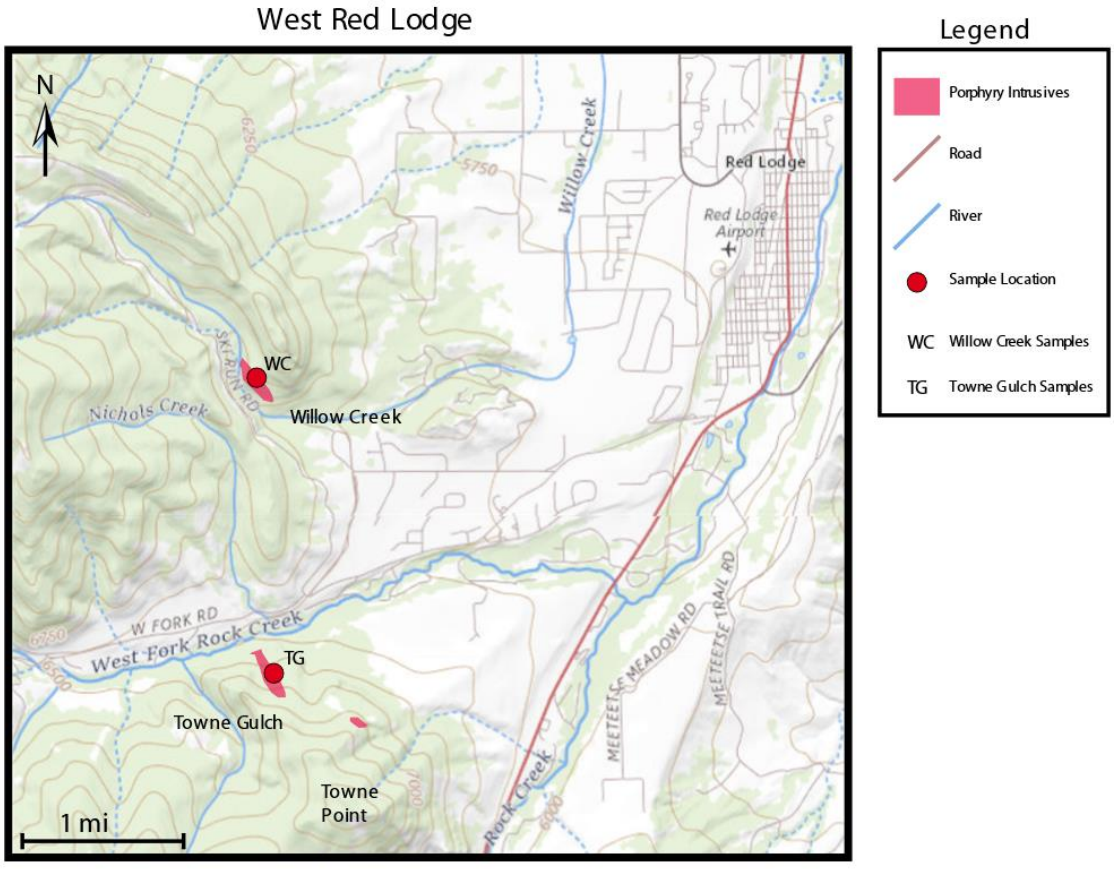

Figure 7 Area west of Red Lodge. Geologic contacts based on maps from Rouse et al. (1937) and Van Gosen et al. (2000).

Tear Fault as well as several minor faults which activated during overthrusting (Rouse et al., 1937; Dutcher et al., 1986).

The Willow Creek outcrop intrudes the near-vertical Gros Ventre shale and lies adjacent to a mafic basement exposure (personal communication from Paez Reyes, 2019). *LF-WC-* samples were collected a year later when conditions were more wet and the area was severely overgrown, obstructing the view of any other units or structures. They were all found on the slope of a small hill. The outcrop appeared to be dark grey because the rocks were wet and covered in lichen. Outcrop was found by locating piles of broken-off rock and walking up the hill from those points. Float was much more prevalent than the actual outcrop. Due to the heavy weathering, good samples were somewhat difficult to find. They consisted of porphyry intrusions with xenolith inclusions of shale (Figure 8 and 9).

Figure 8 Willow Creek samples in outcrop. The image on the left has xenoliths (Paez Reyes, personal communication 2019).

The rocks are a light grey color and zoning is visible in many plagioclase phenocrysts even in hand sample (Figure 6). The rock is primarily groundmass with euhedral plagioclase phenocrysts. The groundmass is too fine grained to allow for identification. Almost all the plagioclase is severely altered, but zoning is still apparent. Smaller anhedral to euhedral biotite

phenocrysts are common and, in some cases, altered to chlorite. Hornblende and quartz phenocrysts are also present, although they are smaller and sparse. Rouse et al. (1937) classified these intrusives as quartz monzonite, however they are severely altered and aphanitic, therefore the classification diagram used in this study is based only on trace elements for volcanic rocks. Using this method, these intrusives are andesite porphyries.

There are two xenolith inclusions in samples from this location as shown in Figures 8 and 9. The triangular xenolith in Figure 8 is a shale. There has been some speculation that it was clay created by the normal fault that the intrusive magma likely traveled through during emplacement. However, this is unlikely as it was lithified and had distinct sharp edges. It is mostly made up of

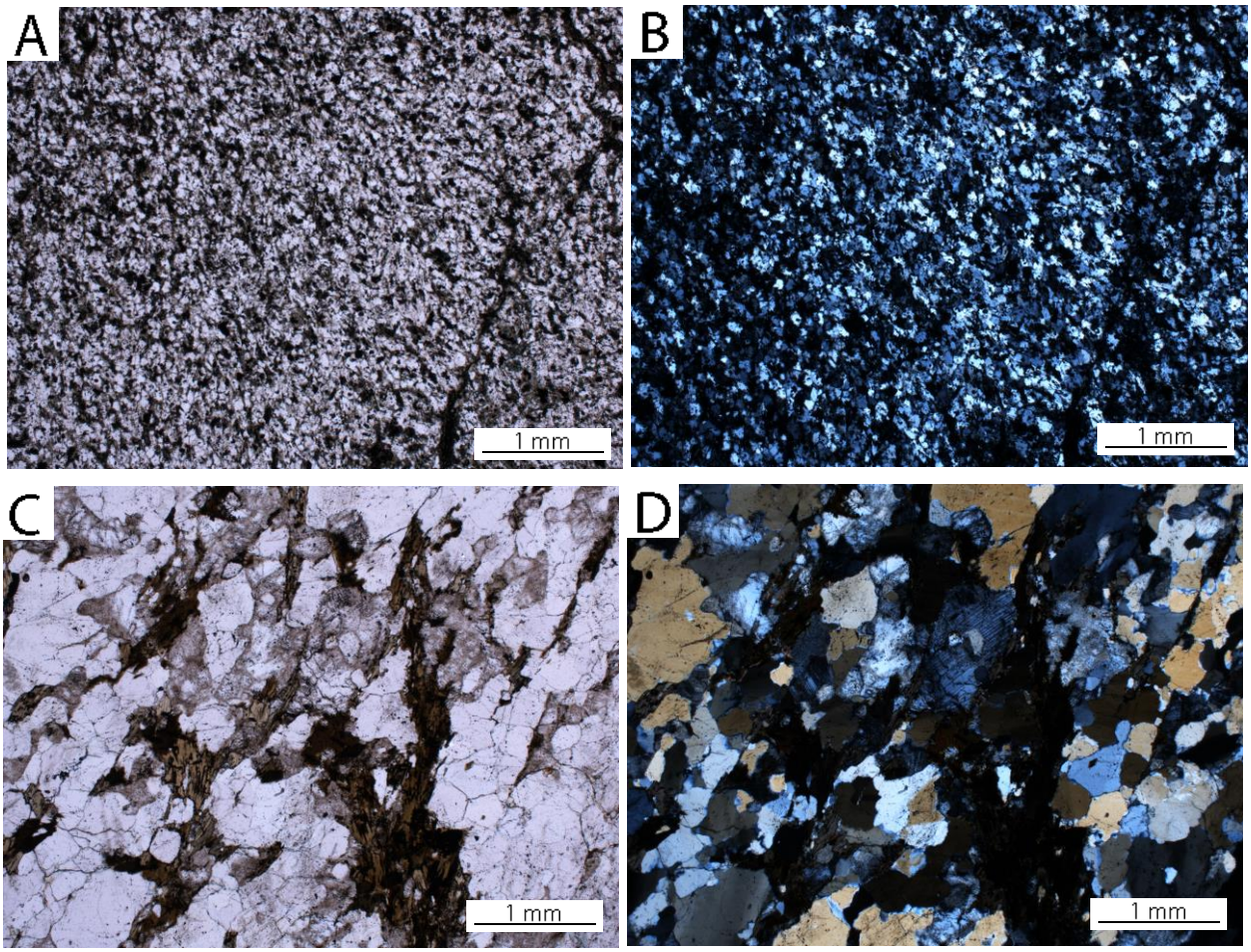

Figure 9 Photomicrographs of xenoliths in the Willow Creek samples shown in both PPL (left) and XPL (right). The upper images are shale and the lower images are quartz feldspar biotite gneiss.

strained quartz. We believe that it most likely belongs to the Woolsey shale (Cambrian). The other is quartz feldspar biotite gneiss. It is made up of strained quartz, biotite, and plagioclase. Some of the plagioclase is sericitized. We believe that this is the Precambrian basement.

2.1.2 Switchbacks

The Switchbacks refers to an area of the Beartooth Highway (US Route 212) southwest of Red Lodge leading up to Beartooth Pass (Figure 10). Samples were taken from three locations in this area including near Quad Creek (sample S2 and S3), along a walking path at the scenic Overlook (sample ABP), and what I refer to in this paper as "Switchbacks 1" (sample S1) as there are no convenient landmarks nearby.

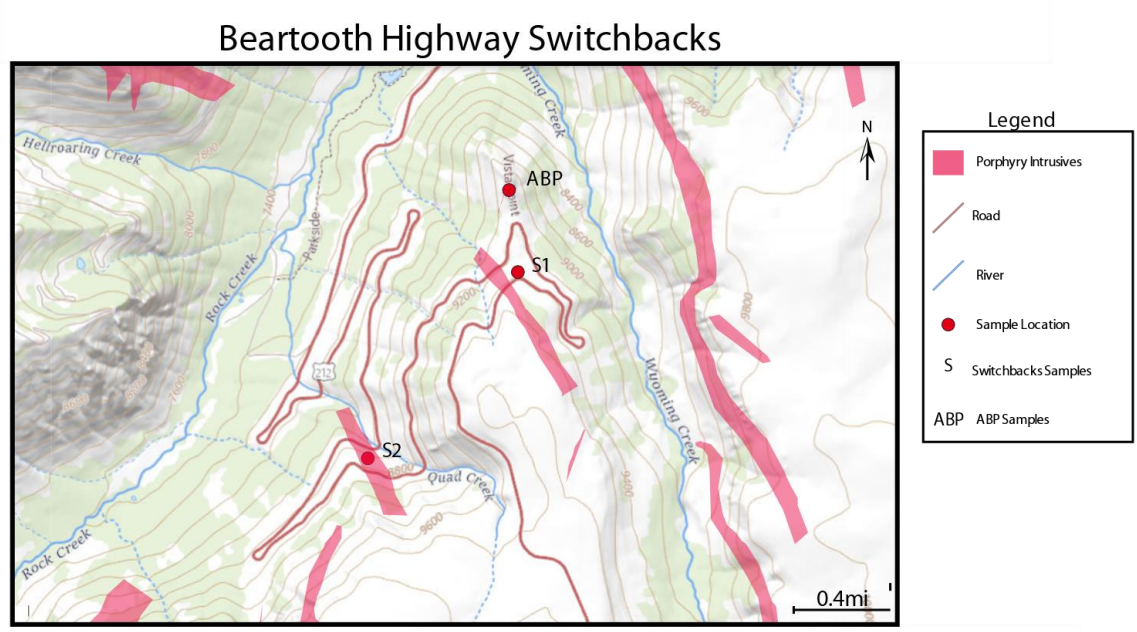

Figure 10 Map of the Beartooth Highway Switchbacks. Geologic contacts are based on Van Gosen et al. (2000). Base map from USGS topographic map.

The Quad Creek outcrop appears to be slightly pink orange in color and is very prominent. Quad Creek samples very closely resemble the samples from the Switchbacks 1

location, but with a brown to pink groundmass. *LF-S-2-* and *LF-S-3* samples were also found in outcrops right along the side of the road. The color is more like Overlook samples, although the matrix is more uniform, and the plagioclase grains are larger. These intrusions were also heavily fractured, and the ground was covered in fractured pieces. Weathered faces are slightly darker in color.

Phenocrysts in this rock include plagioclase, quartz, biotite, and opaque minerals such as hematite. Many of the opaque minerals are euhedral. These intrusions seem to have a larger amount of fracturing and alteration, which has obscured zoning in some cases. Phenocrysts are smaller than those in intrusives from the Red Lodge Front and there is more variety. Biotite and chlorite are not present. Quad Creek intrusives are on the boundary of trachyte and trachyandesite according to Figure 18.

The Overlook outcrop appears to be slightly pink orange in color and is very prominent. It is in place along most of the trail leading to an outlook point from a parking lot along the Switchbacks. It occurs along most of the trail out to a US Forest Service visitor overlook. It is more coarsely grained than the other porphyry intrusives in this study, though the groundmass is still microcrystalline.

This intrusive is similar to the Quad Creek rocks in that they both commonly have opaque minerals. In this rock, however, the opaques tend to be smaller. Alteration in the plagioclase phenocrysts is much heavier on the outer edges and although fractures are common, the centers of the larger grains are relatively clear. Small rounded quartz grains are common. Biotite and chlorite are absent. Although in hand sample Overlook samples appear quite different from Quad Creek, both intrusives lie on the border between trachyte and trachyandesite.

Switchbacks 1 samples were collected on the switchbacks of Beartooth Highway near the Overlook samples. *S1* samples were right along the side of the road at turns. The intrusive shown just to the west were not observed. This does not appear to connect to the Overlook sill. Some orange lichen was on the surface, but for the most part relatively fresh faces were common. These faces were light grey in color and the plagioclase grains were clearly visible apart from the matrix. The rock was fractured heavily and because the unit was cut by the road, was being eroded causing fractured pieces to cover the ground between the road and the outcrop. Here the porphyries occur as sills with thicknesses of 50 to several hundred feet and dips of nearly horizontal to about 30 degrees and have prominent jointing (Stobbe, 1953).

The main phenocryst in these rocks are zoned plagioclase. The grains are usually euhedral and tend to be less altered than in other intrusives described here. Rounded and embayed quartz phenocrysts are common. Biotite phenocrysts are common and, in many cases, have been replaced partially by chlorite. There are some rare pyroxene grains. This is trachyandesite porphyry.

2.1.3 Summary

Several other studies have identified other outcrops of porphyry intrusives in the Beartooth Mountain area. Although these occurrences were not sampled for this study, it is still important to try to identify relationships between them. The porphyry intrusives from different localities vary somewhat, but Rouse et al. (1937) suggests that they are all very similar rock types. They all consist of plagioclase phenocrysts in a felsic groundmass and seem to all be late Cretaceous in age. Across all the locations noted in Rouse et al. (1937), the plagioclase phenocrysts range in composition from Ab90An10 to Ab70An30. The normative plagioclase

varies from Ab100An0 to Ab89An11. The main difference between the intrusives is the presence or lack of quartz phenocrysts.

2.2 Isotopic Geochronology

U-Pb analysis was completed *in situ* using thin sections. The zircon grains were identified using a petrographic microscope in transmitted and reflected light. LA-ICPMS (varian), rep rate = 10 Hz, burst count = 300 shots, fluence = 3.95 J/cm^2, spot size = 25 um/ 15um, energy setpoint = 5.00 mJ, pressure = 6046 mbar, voltage = 15.40 kV. An average of ten grains were analyzed for each location.

2.2.1 Preliminary Research from Shaulis

Barry Shaulis carried out his own geochronology research prior to this study. He collected in an area by the West Fork of Rock Creek near Red Lodge (N 45 09’05.26” W 109 18’53.26”) referred to in this paper as Towne Gulch (TG in figures) and shown in Figure 7. Shaulis analyzed his samples using a new wave 213 nm laser coupled with Nu Plasma HR MCICPMS, 5Hz, 30-micron spot size, ~3.4 J/cm^2 (57% power).

The weighted average 206/238 age was determined using both laser ablation and TIMS methods for the rims of the zircon grains. Laser ablation (n=10) achieved an age of 93.7 +/- 1.1 Ma. The TIMS method resulted in an age of 93.4 +/- 0.5 Ma. These results have good agreement

Preliminary U-Pb Data

	207Pb/ 206Pb	2σ	207Pb/ 235U	2σ	206Pb/ 238U	2σ	ρ	206Pb/238U Age (Ma)	2σ	207Pb/235U Age (Ma)	2σ	207Pb/206Pb Age (Ma)	2σ	206Pb/204Pb Age (Ma)	U	Th	U/Th	204Pb CPS	206Pb CPS
Towne Gulch																			
2014BS3-1	0.2015	0.0021	15.45	0.30	0.549	0.012	0.90	2821	51	2842	18	2843	9	3786	103	98	1	16	60578
2014BS3-2	0.2706	0.0017	24.87	0.42	0.661	0.014	0.98	3270	55	3302	16	3311	6	29732	456	305	2	11	327056
2014BS3-3	0.1969	0.0018	14.12	0.24	0.519	0.010	0.90	2695	44	2761	19	2796	10	5594	135	193	1	14	78318
2014BS3-4	0.1980	0.0043	14.42	0.38	0.527	0.012	0.70	2726	52	2775	25	2792	21	1497	38	20	2	15	22458
2014BS3-5	0.1817	0.0018	12.56	0.22	0.494	0.010	0.56	2588	41	2648	16	2672	12	7267	173	159	1	13	94467
2014BS3-6C	0.1791	0.0028	12.11	0.23	0.487	0.010	0.42	2560	44	2614	17	2659	20	9151	85	54	2	5	45756
2014BS3-6R	0.0512	0.0028	0.11	0.01	0.015	0.000	0.10	95	2	101	5	316	66	1721	638	75	9	6	10328
2014BS3-7	0.0513	0.0036	0.10	0.01	0.014	0.000	0.02	93	3	99	7	319	78	405	485	25	19	19	7695
2014BS3-8	0.2008	0.0030	14.95	0.27	0.535	0.011	0.73	2770	53	2811	17	2839	12	2476	51	25	2	12	29714
2014BS3-9	0.0488	0.0025	0.10	0.00	0.015	0.000	-0.05	93	2	99	4	241	51	872	663	61	11	12	10464
2014BS3-10	0.0542	0.0041	0.11	0.01	0.015	0.000	0.24	94	3	107	8	520	100	634	160	7	24	4	2535
2014BS3-11C	0.2321	0.0034	19.07	0.35	0.594	0.014	0.91	3004	55	3044	18	3060	16	4186	47	41	1	7	29304
2014BS3-11R	0.2029	0.0034	15.42	0.30	0.545	0.011	0.26	2804	44	2843	19	2847	19	6651	67	81	1	6	39908
2014BS3-12	0.2452	0.0015	21.75	0.53	0.638	0.018	0.90	3177	70	3170	23	3154	6	28533	486	64	8	11	313859
2014BS3-13C	0.2377	0.0029	19.50	0.31	0.588	0.011	0.76	2983	46	3066	15	3117	13	6483	100	43	2	10	64830
2014BS3-13R	0.0556	0.0033	0.12	0.01	0.015	0.000	0.61	97	2	111	6	438	75	517	504	12	40	16	8276
2014BS3-14	0.2040	0.0018	14.84	0.32	0.528	0.013	0.63	2733	54	2807	21	2851	10	21912	308	98	3	8	175293
2014BS3-15	0.1951	0.0044	14.14	0.33	0.527	0.012	0.22	2734	49	2757	22	2789	24	1743	37	49	1	12	20910
2014BS3-16	0.2596	0.0014	23.30	0.28	0.647	0.012	0.59	3218	47	3240	12	3243	4	77791	1355	721	2	12	933490
2014BS3-17	0.2013	0.0027	14.77	0.30	0.532	0.011	0.72	2747	47	2799	20	2831	16	2464	47	42	1	11	27106
2014BS3-18	0.0508	0.0029	0.10	0.01	0.014	0.000	0.21	91	2	97	5	327	65	736	565	134	4	12	8827
2014BS3-19	0.2008	0.0057	14.48	0.60	0.520	0.012	0.74	2697	53	2774	39	2815	42	7141	87	40	2	7	49984
2014BS3-20	0.2598	0.0020	22.55	0.38	0.630	0.014	0.61	3149	54	3209	17	3245	8	28237	338	264	1	8	225899
2014BS3-21R	0.2756	0.0020	24.71	0.30	0.646	0.012	0.34	3213	48	3297	12	3334	8	12449	429	431	1	24	298764
2013BS3-21L	0.2679	0.0032	23.74	0.40	0.643	0.013	0.85	3199	52	3257	16	3288	11	4845	70	21	3	10	48446
2014BS3-22C	0.2352	0.0023	19.58	0.35	0.600	0.013	0.81	3029	52	3070	17	3088	11	4682	92	11	9	13	60867
2014BS3-22R	0.0517	0.0024	0.10	0.01	0.015	0.000	0.22	93	2	100	5	317	74	1566	1010	39	26	10	15660
2014BS3-23	0.2750	0.0017	24.88	0.36	0.655	0.013	0.92	3247	49	3303	14	3334	5	11029	222	177	1	14	154402
2014BS3-24	0.2668	0.0019	23.44	0.31	0.633	0.012	0.55	3163	48	3245	13	3285	9	10874	299	234	1	19	206607
2014BS3-25	0.2024	0.0016	15.17	0.21	0.541	0.011	0.89	2787	45	2826	13	2844	9	46099	327	348	1	4	184395
2014BS3-26	0.2691	0.0059	24.15	0.74	0.653	0.016	0.90	3238	64	3259	39	3297	22	951	20	14	1	14	13313
2014BS3-27	0.2594	0.0017	21.74	0.28	0.610	0.012	0.63	3068	47	3172	12	3243	4	182544	278	136	2	1	182544
2014BS3-28	0.0562	0.0048	0.12	0.01	0.015	0.000	0.04	94	2	111	9	570	110	640	327	7	46	8	5119
2014BS3-29	0.2698	0.0021	23.81	0.44	0.642	0.014	0.69	3198	56	3262	17	3305	8	20451	243	109	2	8	163605
2014BS3-30	0.2347	0.0028	19.11	0.35	0.586	0.013	0.57	2974	52	3046	18	3093	15	4076	71	45	2	11	44838
2014BS3-31	0.2736	0.0018	23.90	0.36	0.635	0.012	0.76	3167	47	3265	15	3325	6	19861	322	187	2	11	218476
2014BS3-32	0.3670	0.0360	1.21	0.19	0.024	0.002	0.93	154	12	774	75	3800	120	22	17	7	3	20	434
2014BS3-33	0.1972	0.0022	13.80	0.21	0.507	0.010	0.41	2645	42	2736	15	2793	10	2316	64	75	1	15	34733
2014BS3-34	0.1986	0.0011	14.47	0.18	0.530	0.010	0.67	2741	42	2781	12	2811	5	35849	700	121	6	11	394334
2014BS3-35C	0.1987	0.0032	14.36	0.32	0.525	0.011	0.75	2729	56	2772	21	2799	18	2505	54	63	1	12	30065
2014BS3-35R	0.0507	0.0037	0.10	0.01	0.015	0.000	0.32	94	2	97	7	296	88	724	509	25	21	11	7964
2014BS3-36	0.2052	0.0015	15.45	0.24	0.547	0.011	0.77	2812	45	2842	15	2867	8	15627	249	39	7	9	140642
2014BS3-37	0.1863	0.0032	13.14	0.30	0.509	0.012	0.87	2652	52	2688	22	2726	14	1940	25	11	2	7	13580
2014BS3-38R	0.2101	0.0028	15.57	0.40	0.538	0.012	0.84	2775	50	2848	25	2898	19	15808	276	52	6	10	158080
2014BS3-38L	0.2133	0.0020	15.28	0.30	0.519	0.011	0.84	2696	47	2834	19	2924	10	11007	237	36	7	12	132081
2014BS3-39	0.1953	0.0020	14.09	0.25	0.523	0.011	0.58	2710	46	2755	17	2796	14	4728	79	82	1	9	42551
2014BS3-40	0.2736	0.0024	22.46	0.33	0.594	0.012	0.97	3005	47	3203	14	3329	9	19594	311	227	1	10	195936
2014BS3-41	0.2563	0.0028	23.93	0.36	0.678	0.014	0.12	3338	52	3265	15	3223	10	12266	87	17	5	5	61328
2014BS3-42	0.2436	0.0014	19.80	0.28	0.590	0.011	0.93	2990	46	3081	14	3143	6	25595	406	163	3	10	255954
2014BS3-43	0.0840	0.0160	0.17	0.03	0.016	0.001	0.46	102	5	153	24	1460	210	46	51	1	59	18	823
2014BS3-44C	0.1978	0.0025	14.01	0.23	0.518	0.010	0.40	2691	42	2750	16	2808	11	7543	97	63	2	7	52804
2014BS3-44R	0.0495	0.0032	0.10	0.01	0.015	0.000	0.28	94	2	94	6	400	120	1304	695	76	9	8	10431
2014BS3-45	0.1976	0.0026	14.11	0.22	0.520	0.011	0.51	2698	47	2756	15	2804	15	2312	80	113	1	18	41607
2014BS3-46	0.1964	0.0012	14.38	0.22	0.534	0.011	0.23	2758	45	2775	15	2815	22	40831	733	207	4	10	408314
2014BS3-47	0.2939	0.0029	27.92	0.43	0.689	0.014	0.89	3378	54	3415	15	3440	8	3247	64	40	2	14	45456

Table 1 Preliminary U-Pb data from Barry Shaulis

and are shown in the Concordia plot in Figure 11.

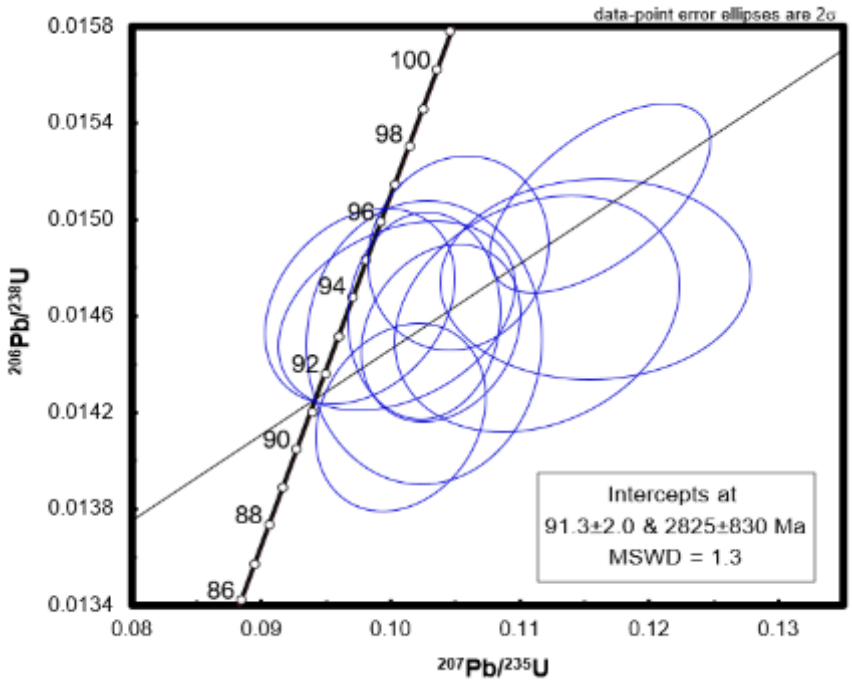

Figure 11 The Concordia plot for the rims of zircon grains. Blue ellipses show individual grains and rims. Thin line shows inherited data. Thick line shows expected Concordia for rims. This data gives an average age of 91 Ma for the dikes.

The age was also determined for the cores of the zircon grains which were produced during a much earlier crystal-forming event and are visible in CL to their rounded edges inside of well-formed zircon grains (Figure 13). Laser ablation (n=55) resulted in cores as old as 3.44 Ga. Using TIMS the oldest age was 3206.6 +/- 2.3 Ma (3.2066 +/- 2.3 Ga). Data from both processes are presented in Figure 11 and 12. These ages correlate with the results of Mueller et al. (1992) and Catanzaro and Kulp (1963) which analyzed zircon grains from an Archean quartzite and metasedimentary rocks in the Beartooth Mountains. They found a predominant age of about 3.3 Ga with a maximum age of 3.96 Ga.

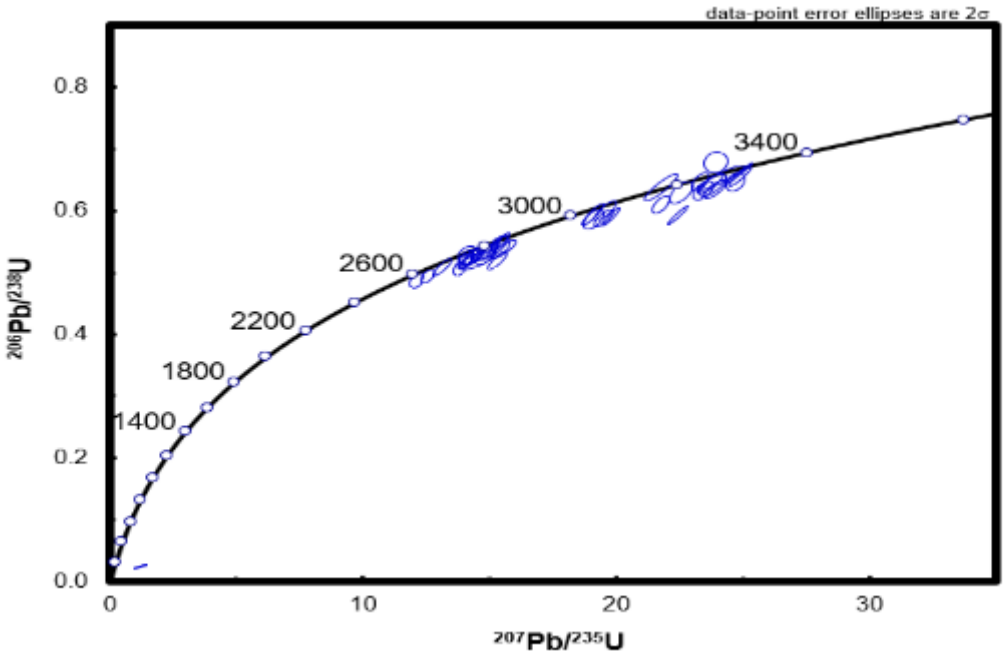

Figure 12 The concordia plot for the cores of zircon grains. Blue ellipses show individual cores. Thick line shows expected concordia for cores. This data shows previous igneous activity in the area.

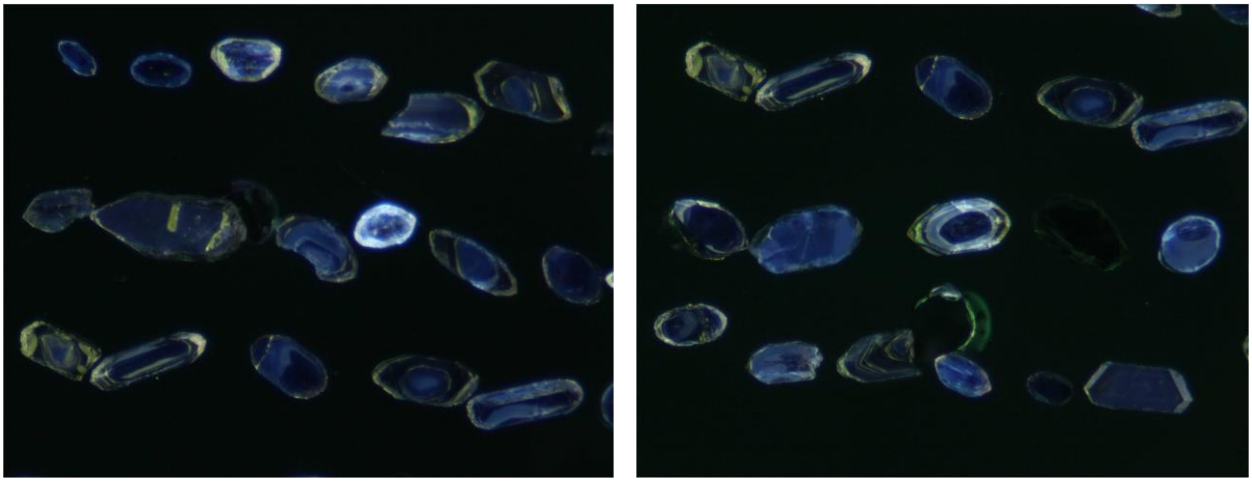

Figure 13 Cathodolumiscence photographs of zircon grains showing rims and cores (Personal communication from Shaulis (2018)).

2.3 Geochemical Techniques

The samples were crushed with a ceramic jaw crusher and powdered with a ceramic shatter box and agate ball mill. They were then processed by the Washington State University GeoAnalytical Lab using both their standard XRF and ICP-MS set-ups. The XRF analysis was done using a ThermoARL Advant'XP+ sequential X-ray fluorescence spectrometer. The powder was prepared by chipping, grinding, weighing with di-lithium tetraborte flux (2:1 flux:rock), fusing at 1000 degrees C in a muffle oven, and cooling before regrinding, refusing, and polishing on diamond laps. ICP-MS analysis was completed by an Agilent 7700 ICP-MS quadrupole mass spectrometer. Samples were prepared using a Cetac ASX-510 auto-sampler and a HEPA filtered enclosure. An all Teflon PFA nebulizer with a quartz, Scott-type, spray chamber was kept at 2 degrees C. The plasma is typically operated at 1250W in this lab. Usual Argan gas flow conditions are as follows: 15 L/min plasma gas, 1 L/min auxiliary gas, 0.8 L/min nebulization gas, and 0.3 L/min make-up gas. Sampling and skimmer cones are made of nickel. In the vacuum region of the Agilent 7700, the positive beam is extracted from the expanding jet, focused, offset by 1 cm, and refocused into a unit mass resolution quadrupole mass filter. Pulse counting at low beam intensities and through current integration at high beam intensities (>3.0 MHz per second) is used for detection by electron multiplier.

3 Results and Discussion

3.1 U-Pb Geochronology

Based on Shaulis' preliminary work, an age of around 93 Ma was expected. The data provided an age of 96.7 +/- 1.7 ma which has good agreement with the preliminary study. This

confirms the late Cretaceous age achieved by Rouse et al. 1937 using relative geochronology. Inherited grains average 106 +/- 44 Ma.

Shaulis extracted zircons and imaged them in cathodoluminescent light in order to analyze specific parts of the zircon grains. He was therefore able to distinguish between inherited cores and the rims which indicate the age of the rocks. My study analyzed the grains in situ without cathodolumiscence imaging. This means that it was not clear what part of the grain I was looking at until the results were processed, giving two distinct ages.

In the Figures 14 and 15, blue data points represent inherited grains and green data represents the age of the intrusive. Data tends to plot linearly rather than on the concordia due to Pb loss. In both Shaulis' study and mine, inherited data is more clustered than colinear because the grains are not all from exactly the same age. It is likely that this study produced a slightly

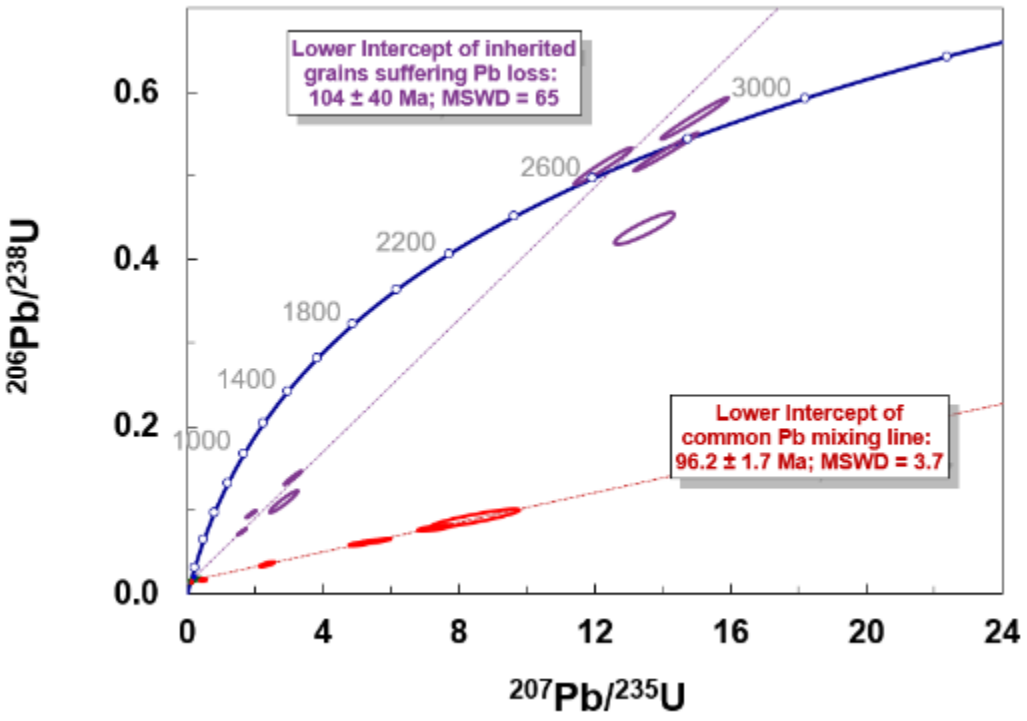

Figure 14 Concordia Plot

older age of new zircon due to the fact that we could not distinguish rims from cores, meaning that some older parts of the grains were possibly included and could have skewed the data making it seem older.

The Terra-Wasserberg plot (Figure 15) exaggerates the intercepts allowing a better view of the true scatter of the data. There is some variation of the 238 to 206 Pb ratio which may suggest that the true intercept is actually a younger age.

If we assume that all of the rocks analyzed in both studies are related, the spread of ages can be attributed to differential Pb loss and to the fact that parts of old zircon may have been averaged into my results. It is also possible that these rocks formed at slightly different times and are less related than previously thought.

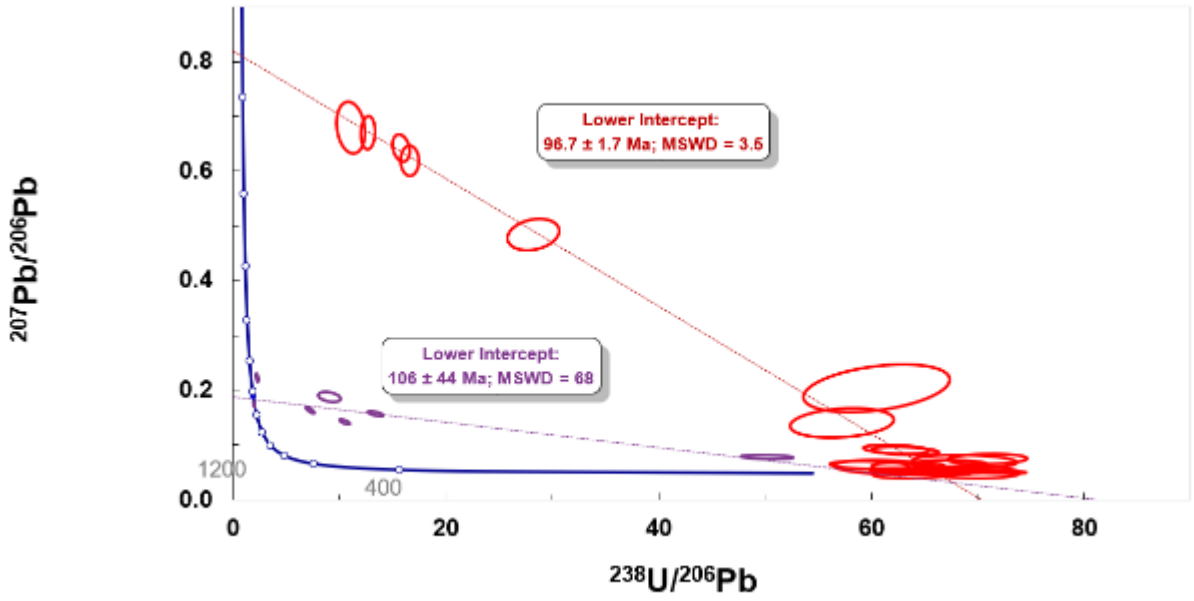

Figure 15 Terra-Wasserburg Plot

U-Pb Data

207Pb/ 206Pb	2σ	207Pb/ 235U	2σ	206Pb/ 238U	2σ	ρ	208Pb/ 232Th	2σ	206Pb/238U Age (Ma)	2σ	207Pb/235U Age (Ma)	2σ	207Pb/206Pb Age (Ma)	2σ	208Pb/232Th Age (Ma)	2σ	U/Th
Switchbacks 1																	
0.14	15.72	0.34	15.77	0.02	6.99	0.23	0.29	21.76	111.78	7.75	296.05	40.49	2233.15	272.09	5139.82	1012.28	69.08
0.20	17.74	0.46	16.74	0.02	9.30	0.17	0.61	32.73	105.85	9.77	387.44	53.92	2856.06	288.78	9598.53	2669.51	26.61
0.05	3.54	0.11	6.20	0.02	3.42	0.89	0.00	14.94	100.16	3.40	101.43	5.98	133.43	83.24	97.31	14.51	22.95
Grove Creek																	
0.05	4.55	0.10	7.06	0.01	3.68	0.82	0.01	33.96	89.80	3.28	95.64	6.44	245.80	104.70	130.46	44.21	73.58
0.68	5.64	8.48	12.54	0.09	10.23	0.90	0.97	10.47	558.69	54.75	2283.58	114.29	4688.59	81.14	13693.1	1068.81	6.79
0.06	3.11	0.12	6.06	0.02	3.55	0.92	0.01	7.39	98.36	3.47	112.91	6.47	433.56	69.38	136.60	10.06	14.47
0.05	3.14	0.10	5.96	0.02	3.70	0.89	0.01	8.87	96.63	3.55	97.81	5.55	128.57	73.87	130.46	11.54	26.38
0.09	6.52	0.20	8.72	0.02	4.07	0.71	0.07	14.24	101.32	4.09	181.28	14.47	1416.34	124.70	1439.12	198.76	36.95
0.05	3.66	0.10	6.00	0.02	3.64	0.82	0.01	12.25	96.80	3.49	100.47	5.73	190.58	85.05	134.63	16.44	30.97
0.62	3.61	5.13	5.60	0.06	4.22	0.77	0.11	2.66	376.57	15.45	1840.40	47.60	4552.17	52.28	2028.39	51.44	1.18
0.67	3.78	7.27	5.57	0.08	4.37	0.74	0.19	3.34	488.80	20.56	2144.89	49.75	4667.15	54.50	3577.95	109.95	1.45
0.64	3.16	5.61	5.78	0.06	4.11	0.85	0.13	3.83	396.20	15.80	1917.92	49.82	4607.50	45.75	2544.43	91.66	1.36
0.16	2.57	3.13	6.70	0.14	4.47	0.97	0.16	2.18	838.21	35.16	1438.88	51.56	2490.86	43.28	2943.29	59.86	2.32
0.05	5.60	0.12	7.59	0.02	4.22	0.69	0.01	66.67	101.45	4.25	113.30	8.13	371.97	126.06	118.19	78.72	102.95
0.48	4.80	2.37	7.44	0.04	6.94	0.78	0.01	3.01	224.76	15.33	1232.34	53.14	4193.28	70.92	265.63	7.94	0.21
0.05	3.07	0.11	5.86	0.02	3.66	0.89	0.01	11.64	99.64	3.62	103.11	5.74	186.06	71.36	116.71	13.55	42.25
0.05	3.16	0.10	5.73	0.02	3.52	0.87	0.00	10.51	97.48	3.41	98.05	5.35	114.09	74.51	99.60	10.45	28.87
0.06	9.65	0.15	11.89	0.02	5.07	0.61	0.01	171.43	107.02	5.38	138.90	15.42	727.22	204.58	155.76	267.76	113.16
0.06	9.49	0.13	10.44	0.02	4.44	0.42	0.07	48.44	100.87	4.44	127.26	12.47	655.27	203.59	1381.31	657.29	126.45
0.09	7.67	0.20	9.67	0.02	4.00	0.65	0.07	14.42	102.74	4.07	187.77	16.56	1462.92	145.83	1406.33	196.82	40.96
0.05	6.33	0.11	7.71	0.02	3.88	0.57	0.01	58.14	98.94	3.81	101.43	7.43	162.42	148.09	191.20	110.94	95.49
0.05	3.59	0.10	5.92	0.01	3.63	0.82	0.01	7.48	95.15	3.43	100.73	5.67	236.89	82.70	113.16	8.44	15.95
0.07	10.42	0.15	10.79	0.01	4.26	0.28	0.02	16.16	90.36	3.82	137.51	13.87	1057.13	209.74	452.82	72.50	14.88
0.06	10.12	0.13	11.18	0.01	4.34	0.43	0.01	23.08	95.19	4.10	126.60	13.30	767.90	213.17	298.44	68.48	12.66
0.05	17.74	0.10	18.98	0.01	5.15	0.37	0.01	142.86	92.08	4.71	97.02	17.55	222.26	410.21	161.25	230.75	72.47
0.05	16.01	0.10	15.68	0.02	5.30	0.11	0.00	1875.00	99.61	5.24	99.26	14.82	92.87	379.17	9.25	174.13	27.88
0.06	27.12	0.13	20.42	0.02	6.44	0.50	0.04	59.38	104.42	6.67	127.48	24.45	583.99	588.82	726.85	428.41	18.63
0.07	31.89	0.14	15.27	0.01	5.89	0.50	0.01	34.19	93.17	5.45	132.56	18.96	914.75	656.15	268.80	91.49	11.45
Inherited Grains (All Grove Creek)																	
0.19	2.11	14.10	5.51	0.53	3.50	0.99	0.16	1.87	2739.30	78.23	2756.15	52.23	2750.67	34.68	2943.29	51.30	0.71
0.14	2.72	1.88	6.21	0.10	3.94	0.95	0.14	2.77	588.57	22.14	1073.29	41.10	2258.85	46.98	2670.33	69.36	5.07
0.17	2.27	12.25	5.56	0.51	3.50	0.98	0.17	2.34	2664.97	76.36	2623.41	52.16	2580.19	37.91	3126.06	67.81	0.79
0.22	1.69	13.47	5.42	0.44	3.52	0.90	0.15	3.85	2339.38	69.15	2713.19	51.25	3006.33	27.20	2764.05	99.61	9.60
0.19	3.95	2.85	11.70	0.11	9.70	0.95	0.21	13.54	675.94	62.27	1369.37	88.10	2718.45	65.04	3889.39	484.88	36.39
0.16	2.23	1.61	5.91	0.07	4.17	0.96	0.10	2.90	464.79	18.72	975.85	37.04	2420.96	37.92	1910.48	52.91	6.53
0.19	1.96	14.95	5.36	0.57	3.55	0.98	0.17	2.25	2903.47	83.10	2812.15	51.01	2749.05	32.21	3201.53	66.84	1.73
0.08	4.17	0.21	6.49	0.02	3.98	0.79	0.04	5.32	127.32	5.02	196.32	11.58	1137.28	82.96	822.91	42.94	18.92

Table 2 Geochronology Data

3.2 Geochemistry

Whole rock and trace element data from eight samples are shown in Tables 3, 4, 5, and 6 (sources are provided in Table 7). Loss on ignition values range from 1.80% to 2.82%. The major element data has been normalized to aid in comparison and analysis. This is possible due to the small range in LOI values and the similar degree of alteration.

Major Oxide Data								
Sample Location	Willow Creek			Switchbacks 1	Grove Creek			Overlook
Sample ID	WC	A2	A4	S1	S2	S2	S3	ABP
Unormalized Oxide wt%								
SiO_2	63.33	63.00	63.76	66.21	66.34	66.37	66.26	67.14
TiO_2	0.29	0.29	0.29	0.21	0.16	0.17	0.16	0.16
Al_2O_3	18.42	18.49	18.62	16.91	17.26	17.12	17.14	16.93
FeO*	3.13	3.15	3.11	1.89	1.47	1.54	1.36	1.41
MnO	0.13	0.13	0.13	0.07	0.06	0.06	0.05	0.06
MgO	1.15	1.33	1.05	0.58	0.18	0.35	0.15	0.20
CaO	2.15	2.33	1.92	3.00	2.25	2.18	2.26	1.86
Na_2O	6.21	5.84	6.44	5.14	5.75	5.77	5.46	5.19
K_2O	3.09	3.25	3.08	2.63	4.06	4.09	4.34	3.66
P_2O_5	0.13	0.14	0.13	0.08	0.05	0.04	0.04	0.05
Sum	98.02	97.93	98.53	96.73	97.58	97.68	97.23	96.65
LOI%	1.80	1.81	1.23	2.82	2.07	2.02	2.52	2.62
Normalized Oxide wt%								
SiO_2	64.61	64.33	64.71	68.45	67.99	67.95	68.15	69.46
TiO_2	0.30	0.30	0.29	0.21	0.16	0.17	0.16	0.16
Al_2O_3	18.79	18.89	18.90	17.48	17.68	17.53	17.63	17.52
FeO*	3.19	3.21	3.16	1.95	1.51	1.57	1.40	1.46
MnO	0.13	0.13	0.13	0.08	0.06	0.06	0.05	0.06
MgO	1.18	1.35	1.07	0.60	0.19	0.36	0.16	0.21
CaO	2.19	2.38	1.95	3.11	2.31	2.23	2.33	1.92
Na_2O	6.33	5.96	6.54	5.32	5.89	5.90	5.62	5.37
K_2O	3.15	3.31	3.12	2.72	4.16	4.19	4.47	3.78
P_2O_5	0.14	0.14	0.14	0.08	0.05	0.04	0.04	0.06
Total	100.00	100.00	100.00	100.00	100.00	100.00	100.00	100.00

Table 3 Major oxide data

The SiO_2 composition ranges from 64.33 wt% to 69.46 wt% across all samples. Samples from locations in the Switchbacks (Switchbacks 1, Quad Creek, and Overlook) have higher SiO_2 contents than those from Willow Creek. Rouse et al. (1937) analyses of porphyry intrusive samples had a similar range of 62.43 wt% to 70.74 wt%, with the Rock Creek sample at 62.43 wt%, Beartooth Plateau from 65.83 wt% to 66.05 wt %, and the Nye Quadrangle at 66.28 wt% to 79.74 wt%. Rouse et al. (1937) does not state the geochemical methods used.

Major oxide data has been plotted on Harker diagrams shown in Figure 21. Data from the general region has been compiled from other published studies as well as from GeoRoc in order to make comparisons. The data is color coded to differentiate between geologic time periods. All geochemical plots use the same legend (see Figure 16).

Major Oxide Data: Rouse et al. (1937)					
Sample Location	Rock Creek	Beartooth Plateau		Nye Quadrangle	
Sample ID	Rock Creek	Timber Creek	Timber Creek	E Round Mtn	NE Round Mtn
Unormalized Oxide wt%					
SiO_2	62.27	65.94	65.74	70.82	66.11
Al_2O_3	17.20	16.79	16.49	15.45	15.44
Fe_2O_3	0.88	1.50	0.66	0.58	1.30
FeO	0.49	0.25	1.01	0.65	1.15
MgO	0.47	0.22	0.83	0.48	0.97
CaO	1.91	2.25	3.33	1.53	2.91
Na_2O	6.07	5.61	4.37	4.52	3.76
K_2O	3.35	4.47	2.35	3.66	3.01
H_2O+	0.63	0.57	1.56	0.99	1.88
H_2O-	0.11	0.22	0.56	0.46	0.47
CO_2	0.91	1.65	2.64	0.55	1.74
TiO_2	0.19	0.20	0.17	0.12	0.27
P_2O_5	0.13	0.06	0.09	0.04	0.67
MnO	0.04	0.09	0.07	0.05	0.06
BaO	0.09			0.22	
Total	94.74	99.82	99.87	100.12	99.74
Normalized Oxide wt%					
SiO2	65.73	66.06	65.83	70.74	66.28
Al2O3	18.15	16.82	16.51	15.43	15.48
Fe2O3	0.93	1.50	0.66	0.58	1.30
FeO	0.52	0.25	1.01	0.65	1.15
MgO	0.50	0.22	0.83	0.48	0.97
CaO	2.02	2.25	3.33	1.53	2.92
Na2O	6.41	5.62	4.38	4.51	3.77
K2O	3.54	4.48	2.35	3.66	3.02
H2O+	0.66	0.57	1.56	0.99	1.88
H2O-	0.12	0.22	0.56	0.46	0.47
CO2	0.96	1.65	2.64	0.55	1.74
TiO2	0.20	0.20	0.17	0.12	0.27
P2O5	0.14	0.06	0.09	0.04	0.67
MnO	0.04	0.09	0.07	0.05	0.06
BaO	0.09	0.00	0.00	0.22	0.00
Total	100.00	100.00	100.00	100.00	100.00

Table 4 Major oxide data from Rouse et al. (1937)

XRF Data								
Sample Location	Willow Creek			Switchbacks 1	Grove Creek			Overlook
Sample ID	WC	A2	A4	S1	S2	S2	S3	ABP
Concentrations in parts per million (ppm)								
Ni	4.2	7.3	6.2	5.6	8.1	10.1	6.0	7.9
Cr	8.1	13.2	9.3	14.4	14.5	18.1	13.5	14.8
Sc	4.2	3.2	3.3	2.9	1.5	2.6	1.9	1.6
V	36.5	36.4	37.5	24.4	22.8	25.7	24.4	18.9
Ba	615	651	542	1054	1042	1131	1484	2254
Rb	87	96	86	93	123	122	130	138
Sr	551	574	563	1267	1154	1288	999	442
Zr	111	110	113	85	123	124	111	101
Y	13.1	12.9	12.7	5.8	5.3	4.7	4.7	5.4
Nb	6.9	6.7	6.6	6.1	7.8	7.1	7.8	6.9
Ga	18.2	19.0	19.4	18.7	19.4	19.5	19.3	18.6
Cu	6.1	4.8	3.3	2.2	1.8	1.6	1.4	1.7
Zn	69.2	68.4	74.9	49.7	38.3	39.0	35.7	49.0
Pb	11.0	12.3	20.3	9.1	13.5	14.4	14.9	15.3
La	17.4	18.8	19.1	8.3	4.9	9.1	5.9	7.7
Ce	34.3	36.8	37.8	12.5	10.7	12.5	9.7	7.7
Th	4.2	4.3	4.4	1.6	1.7	1.6	1.7	1.2
Nd	19.8	21.7	21.3	8.1	6.7	9.4	5.6	6.6
U	1.4	1.0	2.6	2.4	3.0	3.6	3.6	3.1
sum	1617	1698	1583	2671	2602	2844	2880	3101
% of total	0.16	0.17	0.16	0.27	0.26	0.28	0.29	0.31

Table 5 XRF trace element data

ICP-MS Data								
Sample Location	Willow Creek			Switchbacks 1	Grove Creek			Overlook
Sample ID	WC	A2	A4	S1	S2	S2	S3	ABP
Concentrations in parts per million (ppm)								
La	18.46	19.22	20.06	9.19	5.78	6.48	5.38	5.93
Ce	36.94	38.52	40.10	18.83	11.85	13.17	11.13	12.09
Pr	4.71	4.89	5.14	2.44	1.53	1.66	1.45	1.61
Nd	18.95	19.84	20.52	9.83	6.06	6.49	5.70	6.48
Sm	3.69	3.95	3.93	1.87	1.25	1.31	1.17	1.29
Eu	1.25	1.27	1.23	0.59	0.36	0.42	0.39	0.41
Gd	2.80	2.84	2.81	1.26	0.90	1.02	0.86	0.98
Tb	0.39	0.40	0.39	0.17	0.13	0.14	0.12	0.15
Dy	2.21	2.26	2.19	1.00	0.77	0.83	0.75	0.86
Ho	0.44	0.45	0.45	0.20	0.16	0.17	0.16	0.19
Er	1.22	1.23	1.19	0.57	0.48	0.49	0.48	0.54
Tm	0.20	0.19	0.18	0.08	0.08	0.08	0.08	0.09
Yb	1.22	1.25	1.23	0.59	0.52	0.52	0.49	0.63
Lu	0.21	0.20	0.19	0.09	0.09	0.08	0.09	0.11
Ba	625.30	653.00	545.16	1066.00	1049.86	1152.96	1500.20	2286.37
Th	3.78	3.93	4.02	2.14	1.80	1.86	1.76	1.52
Nb	6.75	6.83	6.70	6.69	7.96	8.22	7.89	7.18
Y	12.22	12.29	12.23	5.55	4.83	5.02	4.62	5.30
Hf	2.77	2.83	2.83	2.20	2.95	2.79	2.75	2.48
Ta	0.45	0.49	0.46	0.45	0.45	0.46	0.45	0.45
U	1.76	1.78	1.81	1.39	1.83	1.99	2.41	1.86
Pb	11.27	12.33	20.01	9.24	13.33	14.59	14.88	15.41
Rb	84.38	93.18	84.39	89.09	118.18	119.51	126.69	135.99
Cs	1.48	2.01	1.56	3.04	2.79	2.51	3.50	1.88
Sr	539.03	569.66	559.53	1252.20	1139.54	1290.11	1002.19	439.26
Sc	3.06	3.16	3.02	1.89	1.72	1.89	1.66	1.72
Zr	103.93	107.61	109.56	81.16	112.70	106.04	105.37	98.00

Table 6 ICPMS trace element data

XRF and ICP-MS analyses of trace elements and REEs had good agreement and element data covered by both techniques were averaged in this study. Two classification diagrams are presented. The first is one of the most used geochemical classification diagrams and uses major elements geochemistry. The second uses trace elements. Both are included to allow for comparison, but the trace element classification is favored in this study as the trace elements are less likely to have been altered and is therefore more reliable for these heavily altered rocks. Although these are predominantly fine-grained rocks, Rouse et al. (1937) used a classification scheme for intrusive rocks. Here we have also plotted Rouse et al. (1937) samples and refer to them under the same classification as our samples.

Geochemical Data Sources	
Absaroka	Feeley et al., 2002
	Lindsay and Feeley, 2003
	Feeley, 2003
	Feeley and Cosca, 2003
	Chadwick, 1970
	Condie and Barsky, 1969
	Meen, 1988
	Meen and Eggler, 1987
Beartooth	Condie and Barsky, 1969
	Page and Barnes, 2016
	Jenkins and Mungall, 2018
	Day and Odriscoll, 2019
Big Horn	Condie and Barsky, 1969
Crazy Mountains	Du Bray and Harlan, 1996
	Du Bray et al., 2006
	Dudas 1991
	Dudas 1987
SW Batholiths	Du Bray et al., 2012
	Eaton, 1983
	Mueller et al., 1996
	Sarkar et al., 2009

Table 7 Geochemical Data Sources

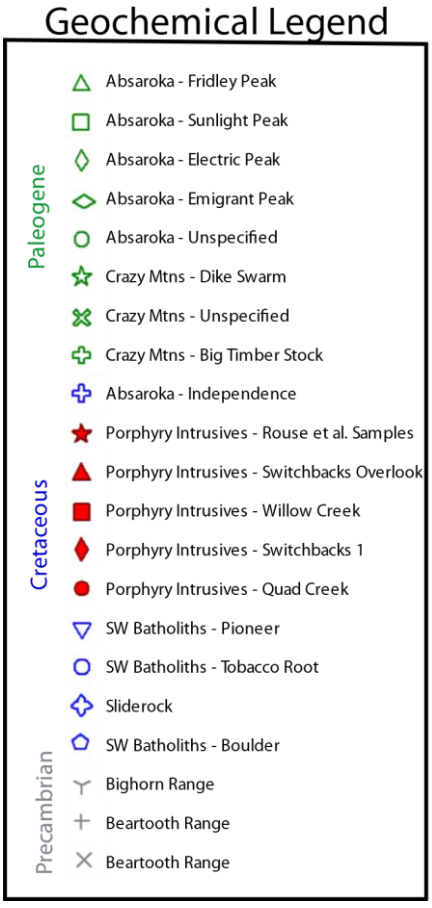

Figure 16 Legend for use with geochemical diagrams

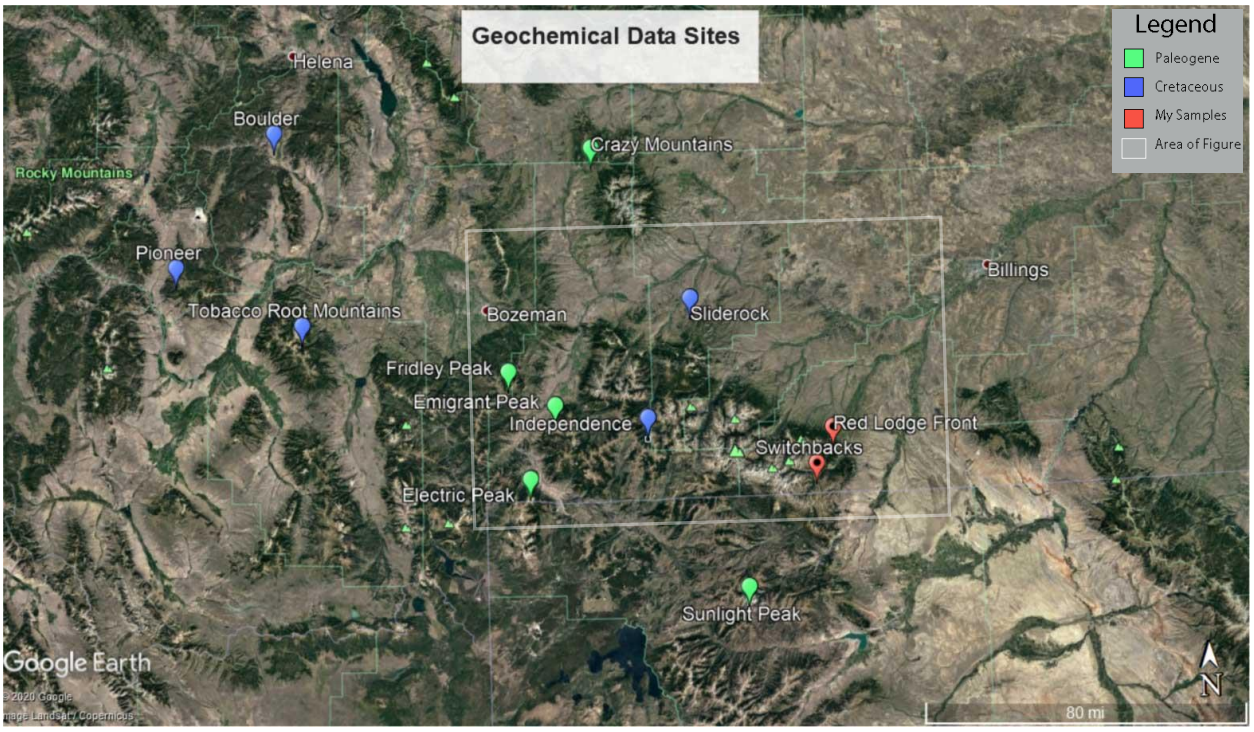

Figure 17 Map showing locations of various geochemical data sites color coded by geologic time period

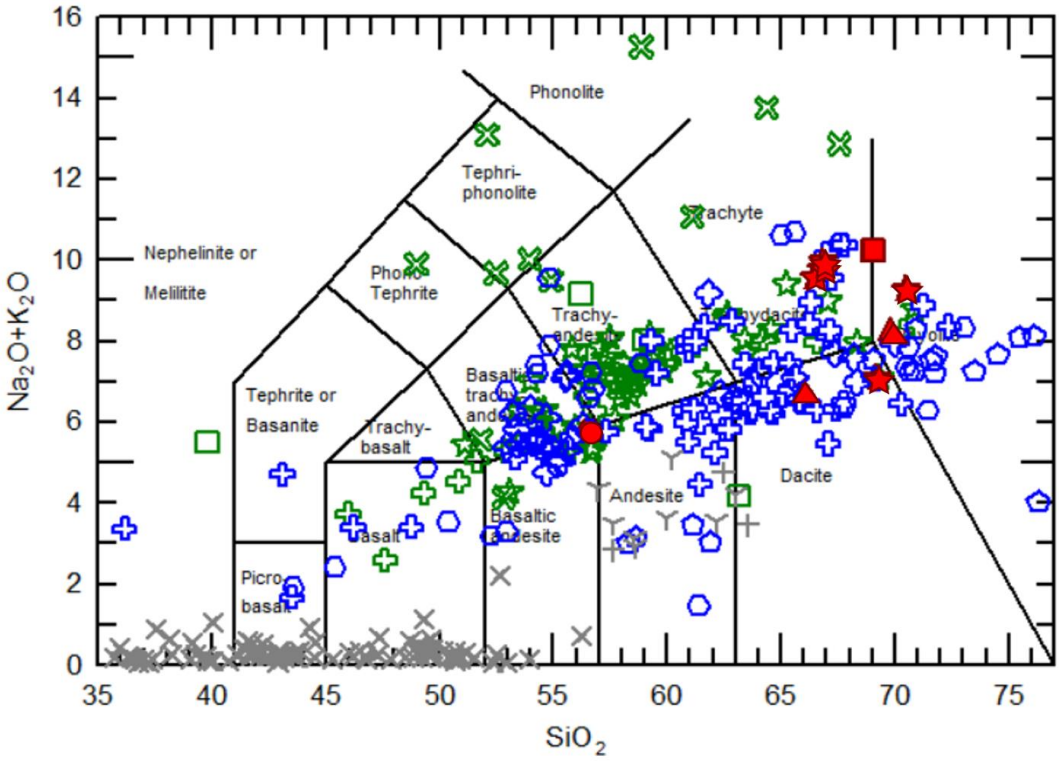

Figure 18 IUGS Classification

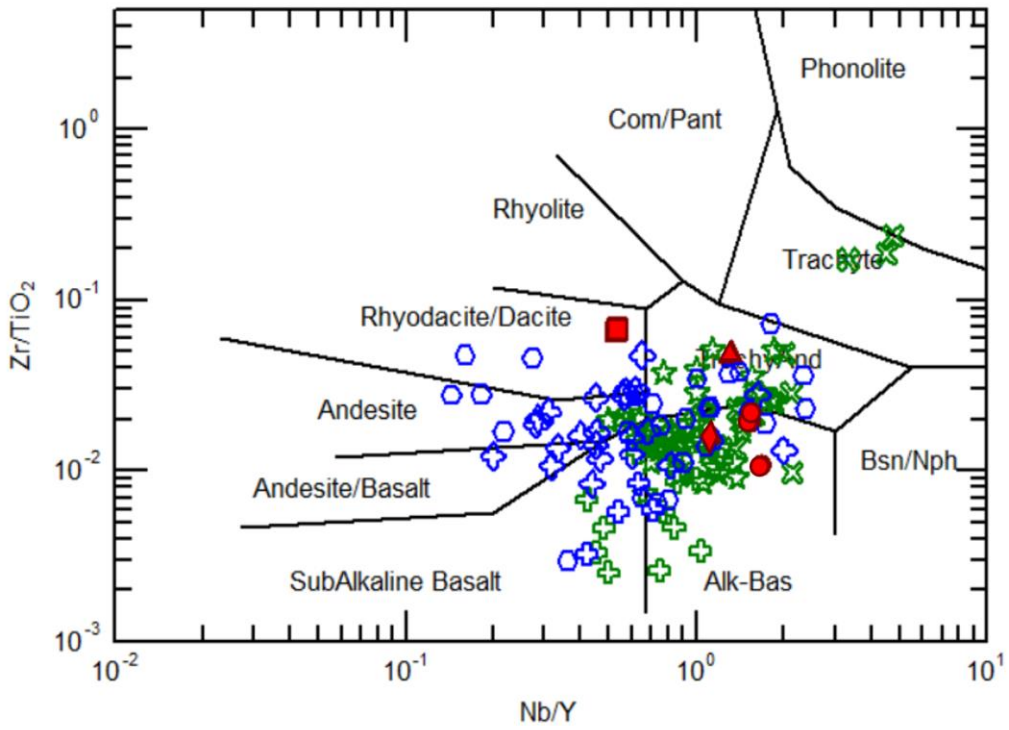

Figure 19 Classification using immobile trace elements: Winchester and Floyd, 1977

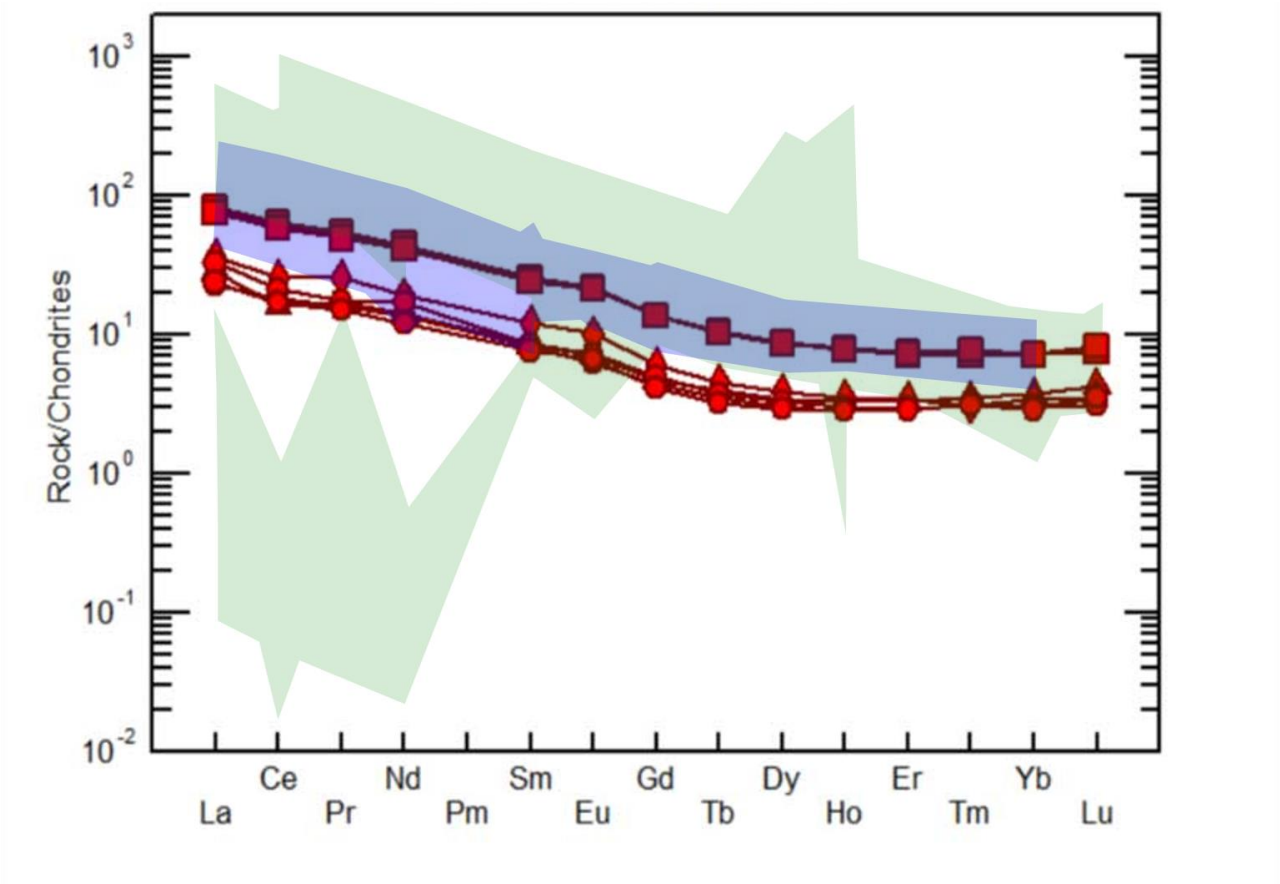

Figure 20 Chondrite-normalized Spider Diagram: Sun and McDonough 1989

Geochemical data is only analyzed on a preliminary basis and a more rigorous study would need to be carried out in order to support the initial observations stated here. Based on these initial graphs, the data is consistent with what would be expected from an igneous series

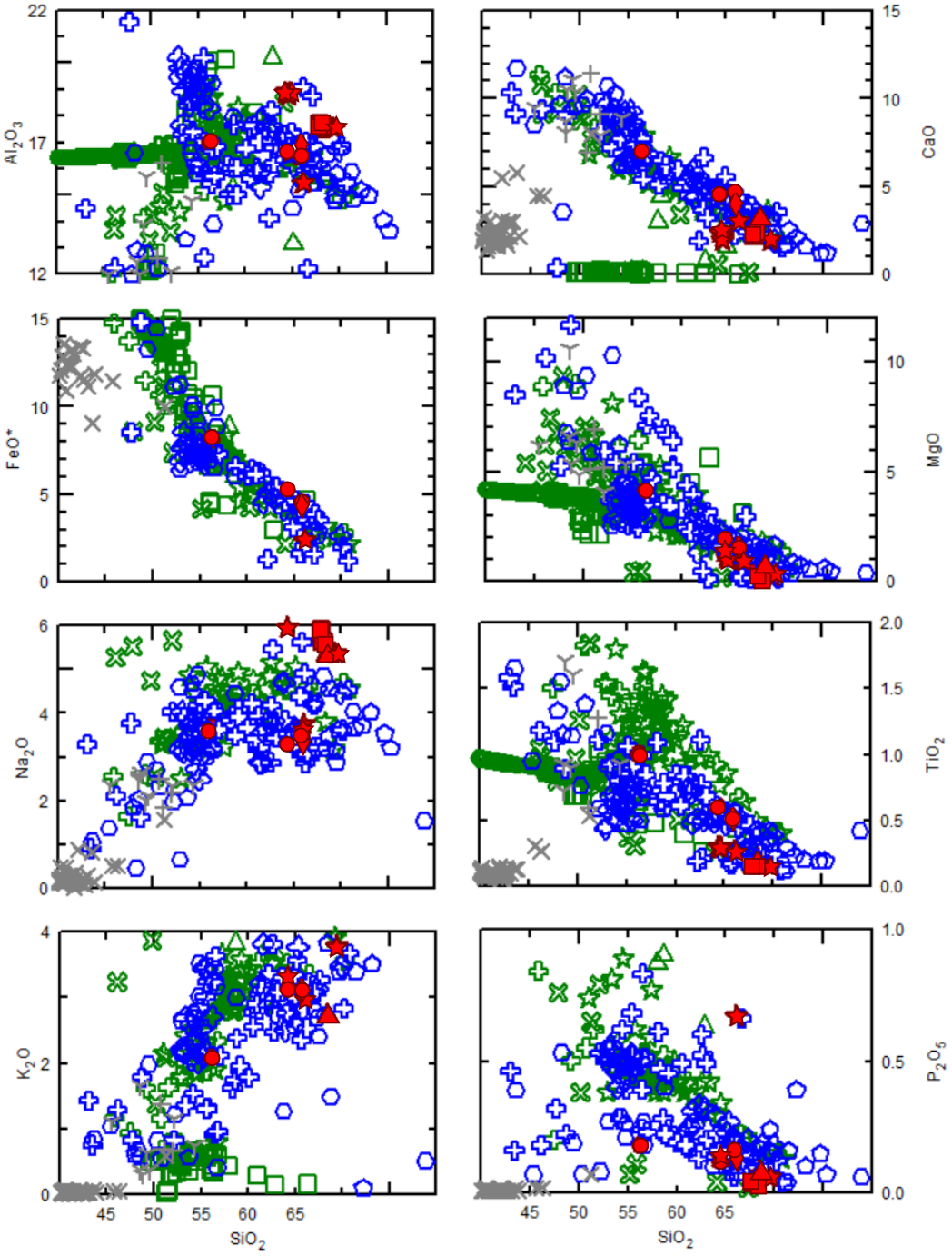

Figure 21 Harker Diagrams

that has gone through fractional crystallization. As shown in the Harker Diagrams of Figure 21, MgO and CaO oxides decrease with increasing SiO2 content and K2O and Na2O oxides increase with increasing SiO2 content. REE patterns are nearly parallel on the Chondrite Spider Diagram (Figure 20). These observations support the fractional crystallization hypothesis; however, they do not prove it. This hypothesis necessitates the assumptions that these rocks were all derived from the same lava, that SiO2 content represents the extent to which the magma evolved, and that fractional crystallization is the sole process involved. It may be noted that the rocks in question do not form perfectly straight lines on the Harker and Fenner diagrams. This may be due at least in part to the porphyritic nature of the rock. Porphyries indicate that the phenocrysts had a longer time to crystallize followed by a shorter period of more rapid crystallization to create the more finely grained groundmass which makes up the rest of the rock. These

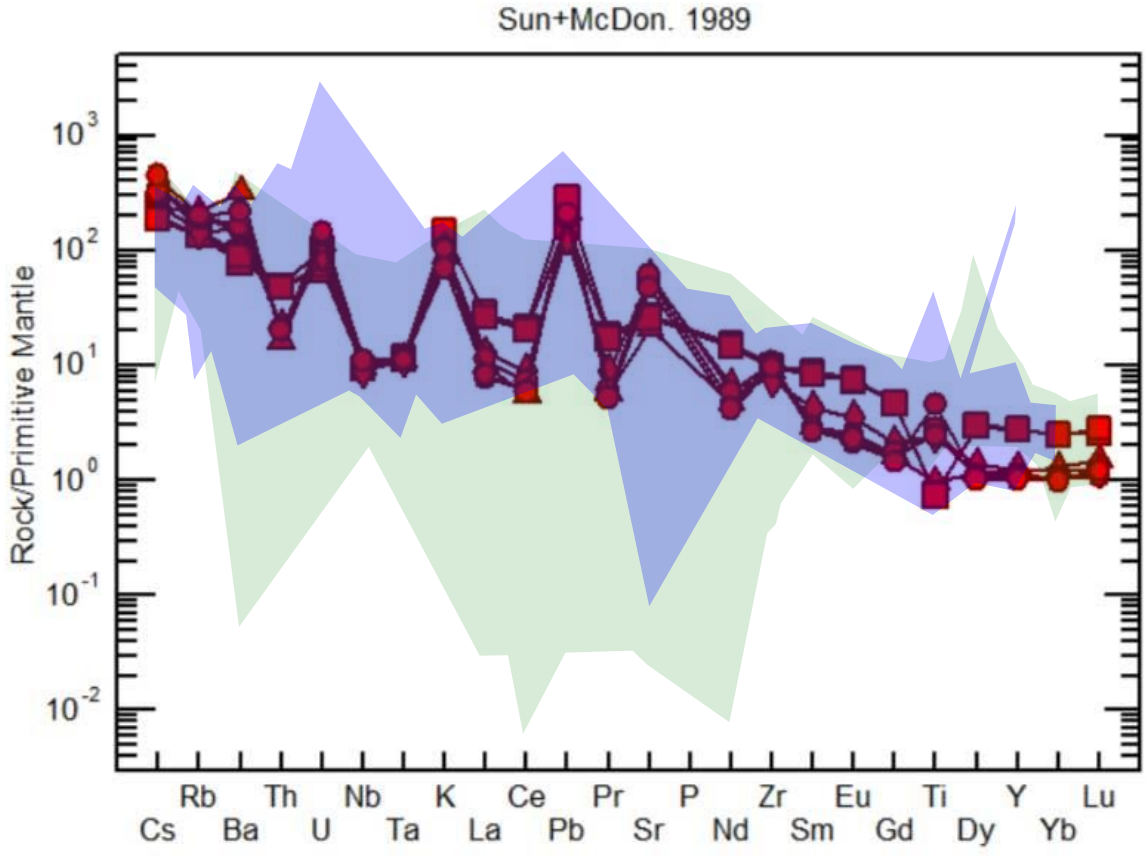

Figure 23 Primitce Mantle Spider Diagram normalized to Sun and McDonough 1989

phenocrysts are included in the data and may have formed under different processes which could throw off the fit on the Harker Diagram. in the data and may have formed under different processes which could throw off the fit on the Harker Diagram.

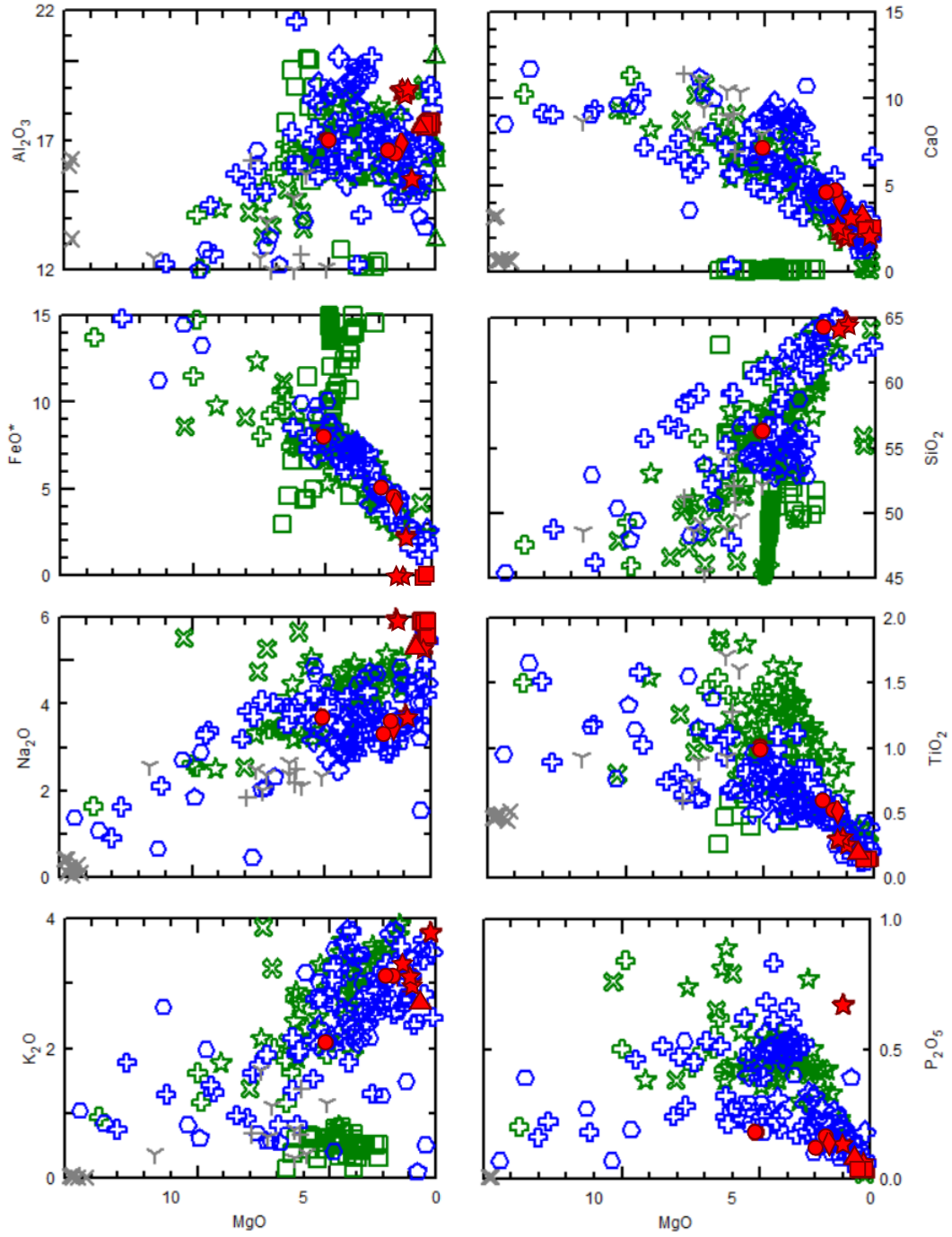

Figure 22 Fenner Diagrams

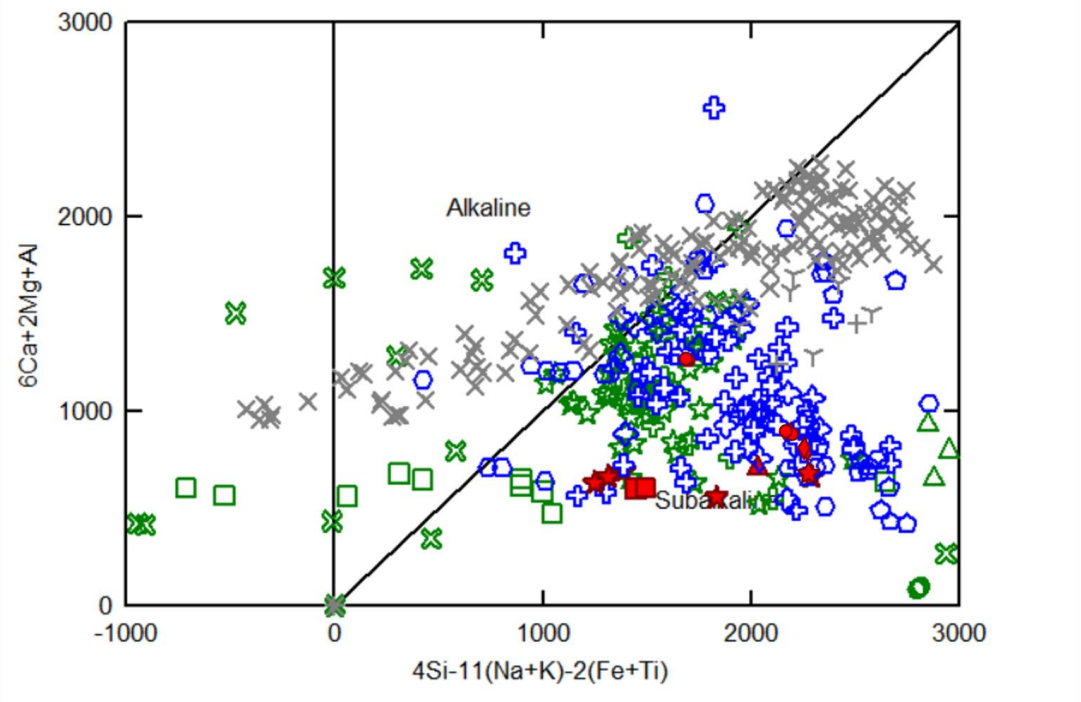

Figure 24 Alkalinity Classification Diagram: De La Roche et al., 1980

3.3 Regional Relations and Cross Section

Based on cross sections from previous studies, and the work done in this study, especially the fact that an inclusion was found in one of the intrusives in the Switchbacks, a general cross section is presented below. This cross section aligns with the contemporary theory that the Beartooth Front is dominantly a horizontal detachment under the basement (Wise, 2000; Berg, 1962; Gries, 1983; Smithson et al., 1978; Erslev, 1993; Allmendinger, 1986; Jordan and Almandinger, 1986; Cook and Varsek, 1994). The lower cross section shows emplacement of the Based on cross sections from previous studies, and the work done in this study, especially the

fact that an inclusion was found in one of the intrusives in the Switchbacks, a general cross section is presented below. This cross section aligns with the contemporary theory that the Beartooth Front is dominantly a horizontal detachment under the basement (Wise, 2000; Berg, 1962; Gries, 1983; Smithson et al., 1978; Erslev, 1993; Allmendinger, 1986; Jordan and Almandinger, 1986; Cook and Varsek, 1994). The lower cross section shows emplacement of the intrusives. Rouse et al. (1937) speculates that there were other sills which were eroded away and others that are still buried beneath those observable today. This is reflected in the cross sections. The top cross section shows the general structure existing today as well as projected units that

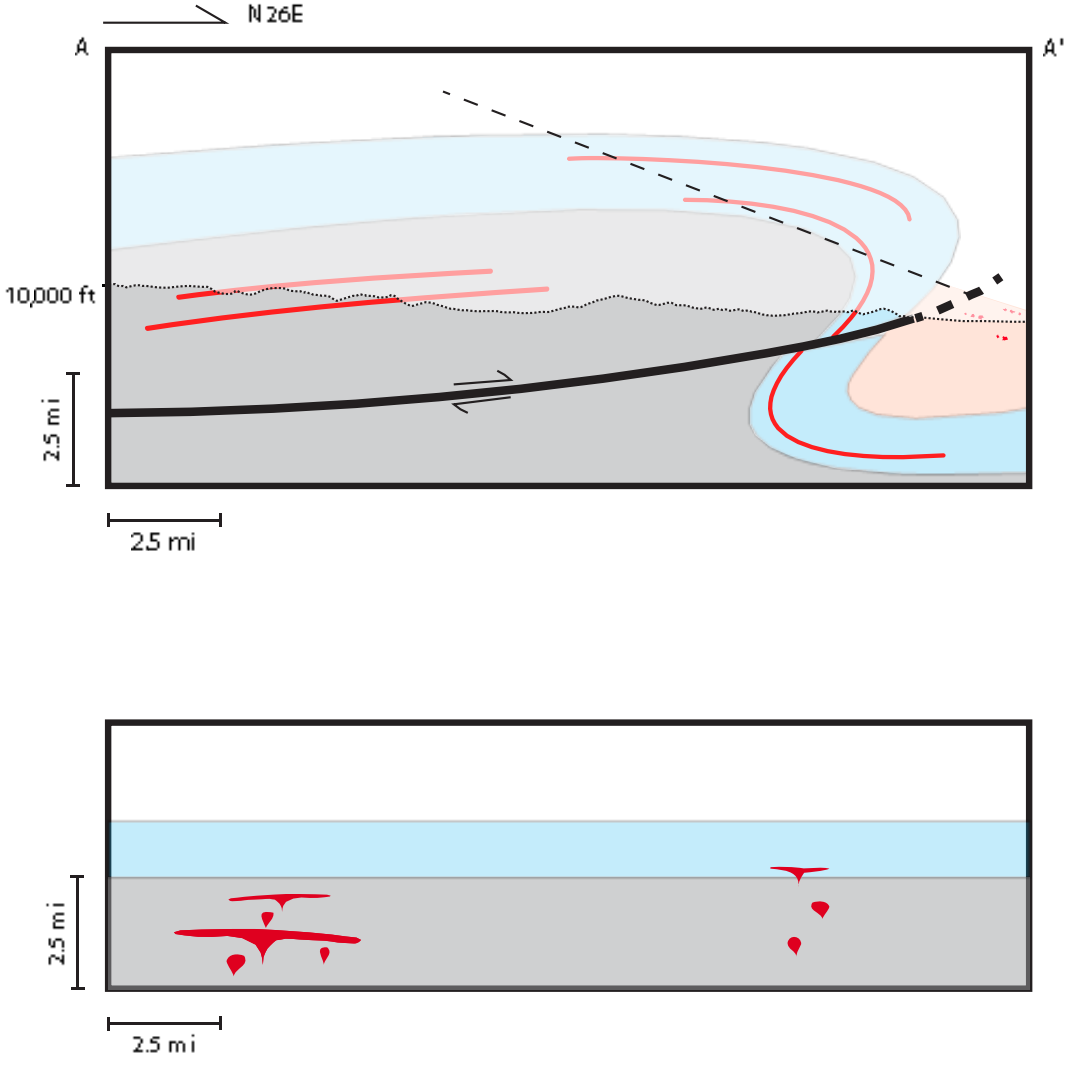

Figure 25 Cross section. The lower figure shows the speculative intrusion while the above figure represents a simplified version of the current state of the rocks.

have since been eroded away. In summary, the porphyries intruded mainly as sills into Precambrian and Phanerozoic rocks which were then faulted and folded by the Beartooth Thrust Fault. Much of the structure has undergone heavy erosion, creating the deposits of the Bighorn Basin which include conglomerates consisting of porphyry intrusives.

Andesitic rocks are generally formed as Continental arcs rather than thrust belts, which is consistent with this study. As discussed previously, these Cretaceous porphyry intrusives were formed prior to main Laramide thrusting, and thus are unrelated to the thrust belt despite their current proximity. Figure 26 provides a general reconstruction of geologic events in the western United States of today. The red square represents my area of study. Although the porphyry intrusives were emplaced are 93 to 97 Mya, this diagram offers interpretations of 100 Ma and 80 Ma. Figure 27 shows cross sections associated with Figure 26. These cover an area south of my area of study but clarify the interaction between the region and the subduction zone to the west. The intrusives of this study are possibly related to the plumes derived from the subducting Farallon plate.

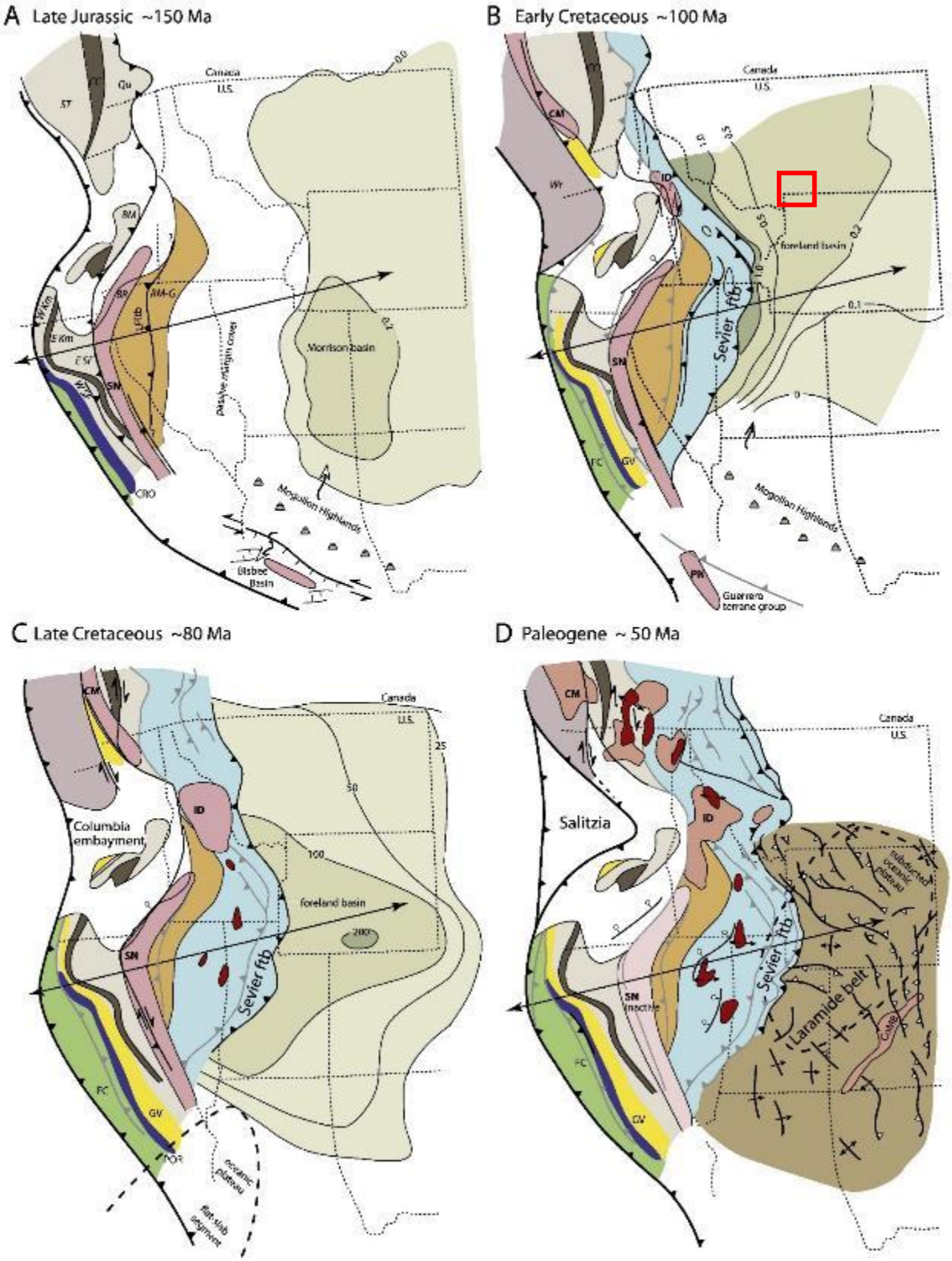

Figure 26 Recreations of the northwestern US. The red square shows the approximate location of the region discussed in this study.

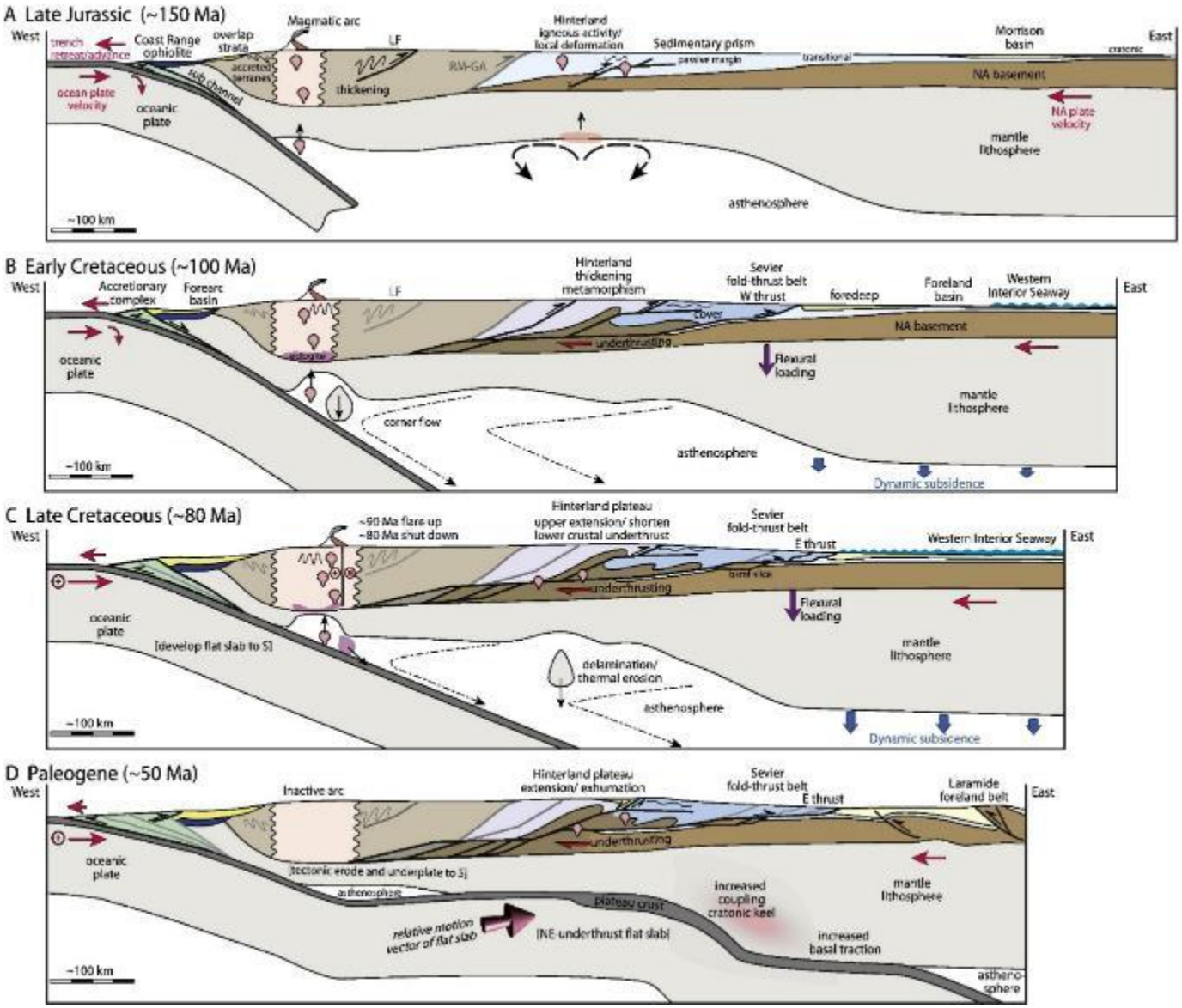

Figure 27 Cross Sections corresponding to Figure 26.

3.5 Further Research

Rouse et al. (1937) posits that there are likely other outcrops of andesite porphyry dikes in the area and gives the locations. It would be beneficial to carry out geochronology on more Cretaceous porphyry intrusives from the area as well as a more in-depth geochemical study. More in depth comparisons of the Cretaceous porphyries of the region would aid in understanding their relation or lack thereof.

4 Conclusion

Cretaceous Porphyry intrusives as first analyzed by Rouse et al. 1937 represent a range in compositions from andesite to dacite. These rocks are part of the late Cretaceous igneous activity which occurred prior to main phase of Laramide thrusting. Rouse et al. (1937) used relative geochronology to conclude that these rocks were late Cretaceous in age. In the decades since then, this has come under dispute as other studies confused them with the Paleogene porphyry intrusives. Barry Shaulis carried out a preliminary study and achieved an age of about 93 Ma from samples near Towne Gulch along the Red Lodge Front and this study aimed to confirm or dispute that age. U-Pb geochronology methods concluded that the porphyry intrusives from the Switchbacks were 96.7 +/- 1.7 ma, achieving good agreement with the preliminary data and conclusions of Rouse et al. (1937). Observations from geochemical data suggest that Cretaceous porphyry intrusives were formed through fractional crystallization. These rocks were likely derived from magmas generated by the subducting Farallon plate to the west.

5 Bibliography

Bartholomew, M., Stewart, K., Wise, D., Ballantyne, H., 2008 Field Guide: Paleoseismites: Indicators of Laramide tectonism and other events near the Bighorn Basin, Montana and Wyoming: The Journal of the Tobacco Root Geological Society, Northwest Geology, v 37, p 135-158

Bevan, A., 1929. Rocky Mountain front in Montana. Bulletin of the Geological Society of America, 40(2), pp.427-456.

Carrapa, B., DeCelles, P.G. and Romero, M., 2019. Early inception of the Laramide orogeny in southwestern Montana and northern Wyoming: Implications for models of flat-slab subduction. Journal of Geophysical Research: Solid Earth, 124(2), pp.2102-2123.

Catanzaro, E.J. and Kulp, J.L., 1964. Discordant zircons from the Little Belt (Montana), Beartooth (Montana) and Santa Catalina (Arizona) Mountains. Geochimica et Cosmochimica Acta, 28(1), pp.87-124.

Chadwick, R.A., 1970. Belts of eruptive centers in the Absaroka-Gallatin volcanic province, Wyoming-Montana. Geological Society of America Bulletin, 81(1), pp.267-274.

Condie, K.C., Barsky, C.K. and Mueller, P.A., 1969. Geochemistry of Precambrian diabase dikes from Wyoming. Geochimica et Cosmochimica Acta, 33(11), pp.1371-1388.

Day, J.M. and O'Driscoll, B., 2019. Ancient high Pt/Os crustal contaminants can explain radiogenic 186Os in some intraplate magmas. Earth and Planetary Science Letters, 519, pp.101-108.

Decelles, P.G., Gray, M.B., Ridgway, K.D., Cole, R.B., Srivastava, P., Pequera, N. and Pivnik, D.A., 1991. Kinematic history of a foreland uplift from Paleocene synorogenic conglomerate, Beartooth Range, Wyoming and Montana. Geological Society of America Bulletin, 103(11), pp.1458-1475.

De La Roche, H., Leterrier, J., Grandclaude, P. and Marchal, M., 1980. A Classification of Volcanic and Plutonic Rocks Using RIR2-Diagram and Major-Element Analyses – Its Relationship with Current Nomenclature. Chemical geology, 29, pp.183-210.

Du Bray, E.A., Aleinikoff, J.N. and Lund, K., 2012. Synthesis of petrographic, geochemical, and isotopic data for the Boulder batholith, southwest Montana (p. 39). US Department of the Interior, US Geological Survey.

Du Bray, E.A. and Harlan, S.S., 1996. The Eocene Big Timber stock, south-central Montana: Development of extensive compositional variation in an arc-related intrusion by side-wall crystallization and cumulate glomerocryst remixing. Geological Society of America Bulletin, 108(11), pp.1404-1424.

Du Bray, E.A., Harlan, S.S. and Wilson, A.B., 2006. Petrology of the Crazy Mountains dike swarm and geochronology of associated sills, south-central Montana (No. 1715). US Department of the Interior, US Geological Survey.

Dudás, F.Ö., 1991. Geochemistry of igneous rocks from the Crazy Mountains, Montana, and tectonic models for the Montana alkalic province. Journal of Geophysical Research: Solid Earth, 96(B8), pp.13261-13277.

Dudás, F.O., Carlson, R.W. and Eggler, D.H., 1987. Regional Middle Proterozoic enrichment of the subcontinental mantle source of igneous rocks from central Montana. Geology, 15(1), pp.22-25.

Dutcher, L.A., Jobling, J.L. and Dutcher, R.R., 1986. Stratigraphy, sedimentology and structural geology of Laramide synorogenic sediments marginal to the Beartooth Mountains, Montana and Wyoming.

Eaton, G.D., 1983. Petrology, petrography and geochemistry of some plutons satellite to the Pioneer batholith, southwestern Montana.

Eckelmann, F.D. and Poldevaart, A., 1957. Geologic Evolution of the Beartooth Mountains, Montana and Wyoming Part 1. Archean History of the Quad Creek Area. GSA Bulletin, 68(10), pp.1225-1262.

Feeley, T.C., Cosca, M.A. and Lindsay, C.R., 2002. Petrogenesis and implications of calc-alkaline cryptic hybrid magmas from Washburn Volcano, Absaroka Volcanic Province, USA. Journal of Petrology, 43(4), pp.663-703.

Feeley, T.C., 2003. Origin and tectonic implications of across-strike geochemical variations in the Eocene Absaroka volcanic province, United States. The Journal of geology, 111(3), pp.329-346.

Feeley, T.C. and Cosca, M.A., 2003. Time vs. composition trends of magmatism at Sunlight volcano, Absaroka volcanic province, Wyoming. Geological Society of America Bulletin, 115(6), pp.714-728.

Foose, R.M., 1958. Structural features of the perimeter of the Beartooth Mountains.

Foose, R.M., Wise, D.U., Fanshawe, J.R., Dutcher, L.A.F., Dutcher, R.R. and French, D.E., 1986. Road Log; Red Lodge to Dead Indian Hill via Clarks Fork Canyon; Tectonics and geologic history of the Beartooth uplift. In Geology of the Beartooth uplift and adjacent basins: Montana Geological Society and Yellowstone—Bighorn Research Associa-tion Joint Field Conference and Symposium (pp. 291-306).

GeoRoc, 2007. GeoRoc, Geochemistry of rocks of the oceans and continents, database. Max-Planck-Institut für Chemie.

Gray, G., Zhang, Z. and Barrios, A., 2019. Basement-involved, shallow detachment faulting in the Bighorn Basin, Wyoming and Montana. Journal of Structural Geology, 120, pp.80-86.

Harms, T.A., Brady, J.B., Burger, H.R. and Cheney, J.T., 2004. Advances in the geology of the Tobacco Root Mountains, Montana, and their implications for the history of the northern Wyoming Province. Special Papers-Geological Society of America, pp.227-244.

Hiza, M.M., 1999. The geochemistry and geochronology of the Eocene Absaroka volcanic province northern Wyoming and southwest Montana, USA.

Hoy, R., Ridgway, K., 1997 Structural and sedimentological development of footwall growth synclines along an intraforeland uplift, east-central Bighorn Mountains, Wyoming: Geological Society of America Bulletin, v 109, no 8, p 915-935

Jenkins, M.C. and Mungall, J.E., 2018. Genesis of the peridotite zone, Stillwater Complex, Montana, USA. Journal of Petrology, 59(11), pp.2157-2189.

Jobling, J.L. and Ritter, D.F., Road Log – Red Lodge, Montana to the East Rosebud River and Return: Tertiary-Pleistocene Stratigraphy along the Beartooth Front.

Jones, W.R., Howland, A.L. and Peoples, J.W., 1960. Igneous and tectonic structures of the Stillwater Complex, Montana. US Government Printing Office.

Koenig, D., 2015. Low-temperature Thermochronology of the Beartooth Conglomerate (Doctoral dissertation).

Le Maitre, R.W. ed., 2004. Igneous rocks: IUGS classification and glossary: recommendations of the International Union of Geological Sciences, Subcommission on the Systematics of Igneous Rock. University of Cambridge.

Lopez, D.A., Sandau, K.L., Thale, P. and Smith, S., 2005. Geologic Map of the Red Lodge Area, Carbon County, Montana. Montana Bureau of Mines and Geology.

Lindsay, C.R. and Feeley, T.C., 2003. Magmagenesis at the Eocene Electric Peak–Sepulcher Mountain complex, Absaroka Volcanic Province, USA. Lithos, 67(1-2), pp.53-76.

May et al., 2013, Detrital zircon geochronology from the Bighorn Basin, Wyoming, USA: Implications for tectonostratigraphic evolution and paleogeography, GSA Bulletin, 125, 1403-1422

Meen, J.K., 1988. Production of isotopic disequilibrium in igneous rocks by crustal contamination—an example from a Laramide volcanic center in Montana, USA. Chemical Geology: Isotope Geoscience section, 72(4), pp.299-309.

Meen, J.K. and Eggler, D.H., 1987. Petrology and geochemistry of the Cretaceous Independence volcanic suite, Absaroka Mountains, Montana: clues to the composition of the Archean sub-Montanan mantle. Geological Society of America Bulletin, 98(2), pp.238-247.

Mudge, M.R., 1968. Depth control of some concordant intrusions. Geological Society of America Bulletin, 79(3), pp.315-332.

Mueller, P.A., Heatherington, A.L., D'Arcy, K.A., Wooden, J.L. and Nutman, A.P., 1996. Contrasts between Sm Nd whole-rock and U Pb zircon systematics in the Tobacco Root batholith, Montana: implications for the determination of crustal age provinces. Tectonophysics, 265(1-2), pp.169-179.

Mueller, P.A., Wooden, J.L. and Nutman, A.P., 1992. 3.96 Ga zircons from an Archean quartzite, Beartooth Mountains, Montana. Geology, 20(4), pp.327-330.

Omar, G.I., Lutz, T.M. and Giegengack, R., 1994. Apatite fission-track evidence for Laramide and post-Laramide uplift and anomalous thermal regime at the Beartooth overthrust, Montana-Wyoming. Geological Society of America Bulletin, 106(1), pp.74-85.

Pagé, P. and Barnes, S.J., 2016. The influence of chromite on osmium, iridium, ruthenium and rhodium distribution during early magmatic processes. Chemical Geology, 420, pp.51-68.

Parsons, W.H., 1942. Origin and structure of the Livingston igneous rocks, Montana. Bulletin of the Geological Society of America, 53(8), pp.1175-1186.

Parsons, W.H., 1958. Origin, age, and tectonic relationships of the volcanic rocks in the Absaroka-Yellowstone-Beartooth Region, Wyoming-Montana.

Paterson et al 2011, Magma addition and flux calculations of incrementally constructed magma chambers in continental margin arcs; Geosphere, 7, 1439-1468

Peccerillo, A. and Taylor, S.R., 1976. Geochemistry of Eocene calc-alkaline volcanic rocks from the Kastamonu area, northern Turkey. Contributions to mineralogy and petrology, 58(1), pp.63-81.

Poldervaart, A. and Bentley, R.D., 1958. Precambrian and later evolution of the Beartooth Mountains, Montana and Wyoming.

Roberts, A.E., 1972. Cretaceous and early Tertiary depositional and tectonic history of the Livingston area, southwestern Montana.

Rouse, J., Hess, H., Foote, F., Vhay, J., Wilson, K., 1937 Petrology, structure, and relation to tectonics of porphyry intrusions in the Beartooth Mountains, Montana: The Journal of Geology, v 45, no7, p 717-740

Rubel, D., 1971 Independence Volcano: A Major Eocene Eruptive Center, Northern Absaroka Volcanic Province: Geological Society of America Bulletin, v 82, p 2473-2494

Sarkar, A., Brophy, J.G., Ripley, E.M., Li, C. and Kamo, S.L., 2009. Geochemical and isotopic studies of the Lady of the Lake Intrusion and associated tobacco root Batholith: Constraints on the genetic relation between Cretaceous mafic and silicic magmatism in Southwestern Montana. Lithos, 113(3-4), pp.555-569.

Schoene, B., 2014 U-Th-Pb Geochronology: Elsavier Ltd, p 341-378

SPENCER, E.W., 1958. Structural trends in the Beartooth Mountains, Montana and Wyoming.

Spencer, E.W., 1959. Geologic Evolution of the Beartooth Mountains, Montana and Wyoming: Part 2. Fracture Patterns. Geological Society of America Bulletin, 70(4), pp.467-508.

Stewart, K., Bartholomew, M., Ballantyne, H., 2008 Laramide paleoseismites of the Bighorn Bas: The Geologic Society of America, Field Guide 10, p 1-15

Stobbe, H., 1952. Porphyry intrusions in the Beartooth Range near Red Lodge. Montana.

Sun, S.S. and McDonough, W.F., 1989. Chemical and isotopic systematics of oceanic basalts: implications for mantle composition and processes. Geological Society, London, Special Publications, 42(1), pp.313-345.

Thornton, C.P. and Tuttle, O.F., 1960. Chemistry of igneous rocks--[Part] 1, Differentiation index. American Journal of Science, 258(9), pp.664-684.

Van Gosen, B.S., Elliott, J.E., LaRock, E.J., Du Bray, E.A., Carlson, R.R. and Zientek, M.L., 2000. Generalized geologic map of the Absaroka-Beartooth study area, south-central Montana (No. 2338).

Vitaliano, C.J., Cordua, W.S., Burger, H.R., Hanley, T.B., Hess, D.F. and Root, F.K., 1979. Geology and structure of the southern part of the Tobacco Root Mountains, southwestern Montana: Map summary. Geological Society of America Bulletin, 90(8), pp.712-715.

Wilson, J.T., 1936. The geology of the Mill Creek–Stillwater area. Montana [Ph. D. dissertation]: Princeton, New Jersey, Princeton University.

Winchester, J.A. and Floyd, P.A., 1977. Geochemical discrimination of different magma series and their differentiation products using immobile elements. Chemical geology, 20, pp.325-343.

Winter, J.D., 2013. Principles of igneous and metamorphic petrology. Pearson education.

Wise, D., 2000 Laramide structures in basement and cover of the Beartooth uplift near Red Lodge, Montana: AAPG Bulletin

Wise, D.U., 2005. Rift and grain in basement: Thermally triggered snapshots of stress fields during erosional unroofing of the Rocky Mountains of Montana and Wyoming. Rocky mountain geology, 40(2), pp.193-209.

Yonkee and Weil 2015; Tectonic evolution of the Sevier and Laramide belts within the North American Cordillera orogenic system, Earth Science Reviews, 150-531-592